



**QUEEN'S  
UNIVERSITY  
BELFAST**

## Exploiting Deep Learning in Limited-Fronthaul Cell-Free Massive MIMO Uplink

Bashar, M., Akbari, A., Cumanan, K., Ngo, H.-Q., Burr, A. G., Xiao, P., Debbah, M., & Kittler, J. (2020). Exploiting Deep Learning in Limited-Fronthaul Cell-Free Massive MIMO Uplink. *IEEE Journal on Selected Areas in Communications*, 38(8), 1678-1697. <https://doi.org/10.1109/JSAC.2020.3000812>

### Published in:

IEEE Journal on Selected Areas in Communications

### Document Version:

Peer reviewed version

### Queen's University Belfast - Research Portal:

[Link to publication record in Queen's University Belfast Research Portal](#)

### Publisher rights

© 2020 IEEE.

This work is made available online in accordance with the publisher's policies. Please refer to any applicable terms of use of the publisher.

### General rights

Copyright for the publications made accessible via the Queen's University Belfast Research Portal is retained by the author(s) and / or other copyright owners and it is a condition of accessing these publications that users recognise and abide by the legal requirements associated with these rights.

### Take down policy

The Research Portal is Queen's institutional repository that provides access to Queen's research output. Every effort has been made to ensure that content in the Research Portal does not infringe any person's rights, or applicable UK laws. If you discover content in the Research Portal that you believe breaches copyright or violates any law, please contact [openaccess@qub.ac.uk](mailto:openaccess@qub.ac.uk).

### Open Access

This research has been made openly available by Queen's academics and its Open Research team. We would love to hear how access to this research benefits you. – Share your feedback with us: <http://go.qub.ac.uk/oa-feedback>

# Exploiting Deep Learning in Limited-Fronthaul Cell-Free Massive MIMO Uplink

Manijeh Bashar, *Member, IEEE*, Ali Akbari, *Member, IEEE*, Kanapathippillai Cumanan, *Senior Member, IEEE*, Hien Quoc Ngo, *Member, IEEE*, Alister G. Burr, *Senior Member, IEEE*, Pei Xiao, *Senior Member, IEEE*, Mérouane Debbah, *Fellow, IEEE*, and Josef Kittler, *Life Member, IEEE*

**Abstract**—A cell-free massive multiple-input multiple-output (MIMO) uplink is considered, where quantize-and-forward (QF) refers to the case where both the channel estimates and the received signals are quantized at the access points (APs) and forwarded to a central processing unit (CPU) whereas in combine-quantize-and-forward (CQF), the APs send the quantized version of the combined signal to the CPU. To solve the non-convex sum rate maximization problem, a heuristic sub-optimal scheme is exploited to convert the power allocation problem into a standard geometric programme (GP). We exploit the knowledge of the channel statistics to design the power elements. Employing large-scale-fading (LSF) with a deep convolutional neural network (DCNN) enables us to determine a mapping from the LSF coefficients and the optimal power through solving the sum rate maximization problem using the quantized channel. Four possible power control schemes are studied, which we refer to as i) small-scale fading (SSF)-based QF; ii) LSF-based CQF; iii) LSF use-and-then-forget (UatF)-based QF; and iv) LSF deep learning (DL)-based QF, according to where channel estimation is performed and exploited and how the optimization problem is solved. Numerical results show that for the same fronthaul rate, the throughput significantly increases thanks to the mapping obtained using DCNN.

**Index Terms**—Busgang decomposition, cell-free massive MIMO, convex optimization, convolutional neural network, deep learning.

## I. INTRODUCTION

Cell-free massive multiple-input multiple-output (MIMO) is a scalable and practical version of network MIMO or coordi-

M. Bashar, P. Xiao are with the Institute for Communication Systems (ICS), the Home of 5G Innovation Centre (5GIC), University of Surrey, GU2 7XH, U.K., e-mail: {m.bashar,p.xiao@surrey}@surrey.ac.uk. and mb1465@york.ac.uk. A. Akbari and J. Kittler are with the Centre for Vision, Speech and Signal Processing (CVSSP), University of Surrey, GU2 7XH, U.K., e-mail: {ali.akbari,j.kittler}@surrey.ac.uk. K. Cumanan and A. G. Burr are with the Department of Electronic Engineering, University of York, Heslington, York, YO10 5NG, U.K. e-mail: {kanapathippillai.cumanan, alister.burr}@york.ac.uk H. Q. Ngo is with the School of Electronics, Electrical Engineering and Computer Science, Queen's University Belfast, Belfast, BT7 1NN, U.K., hien.ngo@qub.ac.uk. M. Debbah is with the Large Networks and Systems Group (LANEAS), CentraleSupélec, Université Paris-Saclay, Gif-sur-Yvette 91192, France, and also with the Mathematical and Algorithmic Sciences Lab, Huawei Technologies Co., Ltd., Boulogne-Billancourt 92100, France. e-mail: merouane.debbah@centralesupelec.fr.

The work of K. Cumanan and A. G. Burr was supported by H2020-MSCA-RISE-2015 under grant number 690750.

The work of H. Q. Ngo was supported by the UK Research and Innovation Future Leaders Fellowships under Grant MR/S017666/1.

The work of P. Xiao was supported by the U.K. Engineering and Physical Sciences Research Council under Grant EP/P008402/2. The authors also would like to acknowledge the support of the 5G Innovation Centre, University of Surrey, U.K. (<http://www.surrey.ac.uk/5gic>) for this work.

Parts of this work was presented at the IEEE ICC 2020 [1].

nated multipoint processing, which synergistically combines massive MIMO technology and cloud radio access networks (C-RAN) [2]–[6]. It has received a lot of research attention for its ability to improve the network connectivity and energy efficiency [7]–[10]. In [7] a user-centric approach is proposed where each user is served by a small number of access points (APs). Moreover, the effect of hardware impairments on cell-free massive MIMO is investigated in [8]. In [11], [12], the authors investigate decentralized schemes for the MIMO systems, which can be applicable to the cell-free massive MIMO. The analysis of favorable propagation and channel hardening in cell-free massive MIMO is presented in [9]. The work in [10], [13] presents a large scale fading (LSF) postcoding vector scheme in cell-free massive MIMO.

One of the main issues for cell-free massive MIMO systems is the limited capacity of the fronthaul links from the APs to the central processing unit (CPU) [14]–[17], or similarly to the edge cloud processor, as described in [18]. Hence a practical combination of the aforementioned technologies is limited-fronthaul cell-free massive MIMO. The limited capacity links from the APs to the CPU constitute one of the most substantial challenges in cell-free massive MIMO [15], [16]. As such, the implementation of cell-free massive MIMO with limited fronthaul links is the main challenge in the uplink mode, as the limited fronthaul links forward the received signal from the APs to the CPU. When converted to digital form this requires a capacity for the fronthaul links many times the corresponding user data rate, to ensure signals are transferred with sufficient precision. In the C-RAN literature this has been estimated as 20-50 times the corresponding data rate, implemented using the common public radio interface (CPRI) standard [19], typically over optical fiber [20].

In limited-fronthaul cell-free massive MIMO, depending how the APs process and forward the signals to the CPU, there are two main types of transmission: combine-quantize-and-forward (CQF) and quantize-and-forward (QF). For CQF, the APs combine the received signals by multiplying them with the conjugate of the channel estimates, and the quantized versions of these combined signals are sent to the CPU for signal detection [15], [16], [21], [22]. While for QF, the APs send the quantized versions of the received signals and the channel estimates to the CPU through limited fronthaul links. Signal combining and detection are then performed at the CPU [17]. The relative performance and the required fronthaul rate of the CQF and QF schemes depend on the number of antennas at each AP, the total number of APs and the channel coherence

time [15]. However, in the QF scheme, since the quantized versions of the received signals and the channel estimates are available at the CPU, zero-forcing (ZF) can be implemented to improve the system performance.

In this paper, we focus on the QF scheme with maximum ratio combining (MRC) and ZF techniques at the CPU. We use the Bussgang decomposition to model the quantized signal. Maximum sum rate power control is investigated. This is the first paper which considers the sum rate maximization problem in limited-fronthaul cell-free massive MIMO. This optimization problem needs to be solved for each coherence interval of the small-scale fading (SSF), which is (mostly) infeasible in real time systems. This practical limitation is a more crucial challenge in cell-free massive MIMO, as the optimization problem should be centrally solved at the CPU, which introduces huge delay. Hence, it is necessary to find a low complexity and practically feasible solution for optimization problems. For this reason we propose to find the optimal power control coefficients based on LSF, which can be calculated much less often. Unfortunately however no closed form expression for the sum rate is available in terms of the LSF coefficients, and hence we formulate an optimization based on the quantized channel estimates, and provide a new heuristic approach to its solution. Finally we use the results from this optimization to train a deep convolutional neural network (DCNN) to determine the power control coefficients based on the LSF. Recently, different machine learning techniques have been exploited to solve challenging research problems in various communications systems my papers and [23]–[28]. In particular, the DCNN has been widely used to design the power elements in the wireless communication networks [26]–[28]. Note that as the DCNN has the ability to reduce the spectral variance in the input features, it is very powerful and the most popular DNN family [29], [30]. Moreover, DCNN reduces the spectral variation in the input signal and can model spectral correlation whereas the fully connected layers aggregate the local information learned in the convolutional layers [29]. Note that the LSF components change very slowly with time. Compared to the SSF, the LSF changes much more slowly, some 120 times slower according to [31], [32]. The contributions of the paper are summarized as follows:

- We provide the achievable rate of the QF scheme for MRC and ZF by treating the quantized versions of the channel estimates as the side information. For the comparison, simple but looser capacity bounds using use-and-then-forget (UatF) bounding technique [33] for both QF and CQF scheme are also provided.
- We propose a sum rate maximization problem taking into account the per-user power constraints and throughput requirement constraints, as well as the quantized channel estimates. This problem is non-convex. Thus, we propose to use a heuristic and useful sub-optimal approach where the original optimization problem is reformulated as a standard geometric programme (GP). The resulting power control algorithm can be applied for all achievable rates of both QF and CQF schemes.

- We propose a LSF-deep learning (DL)-based power control scheme to allocate the power control coefficients in the both QF and CQF schemes using only the LSF coefficients as input. The main idea of the current paper is to train a neural network so that it will derive “optimum” transmit powers for the users using the LSF coefficients as inputs, based on the results of the optimization over a large number of randomly chosen SSF coefficients. The proposed scheme exploits a DCNN to determine an *unknown mapping* between the LSF components and the optimal power obtained by solving the proposed channel-based optimization scheme. The computational complexity of the proposed scheme is presented. In addition, we propose to provide unique inputs for each MRC and ZF receiver which enable the convolutional neural network (CNN) to learn an unknown mapping between the input and the power elements obtained through the convex optimization approach. We show that as our data has a local, spatially invariant structure, we can effectively model it by limiting the connectivity between the successive layers of DNN to local neurons. Furthermore, for the given loss function, we study the error bound. Next, we investigate the case when some users are not active. A novel input matrix is proposed to deal with the non-active users, showing that the proposed DCNN is practical in real-time systems.

There are three important differences between the proposed DCNN-based algorithm in this paper and the scheme presented in [27], which are: (i) In [27], the authors propose to use a deep learning approach to solve an optimization problem which could be solved through the standard convex optimization software. However, the main contribution of our work is finding an unrevealed *mapping* between the LSF components and the power elements obtained using the quantized version of the estimated channel. Note that without the machine learning tool, it is impossible to find a mapping between the LSF coefficients and the optimal power elements which are obtained by solving the sum rate optimization problem with knowledge of the quantized channel (which is a function of SSF coefficients). This is because, given that only the quantized version of the estimated channel is available at the CPU as side information, the sum rate is a function of the SSF. So, it is not possible to explicitly find a mapping between the sum rate and LSF coefficients. This is the main difference between the current work and the work in [27]; (ii) The authors in [27] consider a cellular massive MIMO system, while here we consider a cell-free massive MIMO system. Note that unlike [27], having pure LSF components (i.e., the coefficients  $\beta_{mk}$  defined in (1)) as a raw input of the DCNN does not work in cell-free massive MIMO, and the network cannot learn the power elements obtained through the convex optimization approach. Hence, we generate a novel and unique input matrix to feed as the input to the DCNN for each ZF and MRC receiver. This unique inputs enable the DCNN to learn a *mapping* between the input matrix and the power elements obtained by the convex optimization approach with using the quantized version of the estimated

channel; and (iii) The authors in [27] consider the sum spectral efficiency optimization problem in cellular massive MIMO without considering any spectral efficiency requirements at each user. However, in our work, we take into account the throughput requirement constraints.

Finally, the work of the present paper is different from the recent work [34]. A cell-free massive MIMO with perfect fronthaul is considered in [34], where the authors consider the max-min rate and sum rate optimization problems without having any throughput requirement constraints. Moreover, in [34], the authors find an unknown mapping between the LSF components and the optimal power elements obtained by having the LSF components at the CPU. However, in the present work, we find an unknown mapping between the LSF components and the power elements obtained by the knowledge of the SSF components at the CPU. Finally, in [34], the authors use 2,000,000 training samples to train the neural network whereas having only 60,000-70,000 training examples are enough for our proposed network.

*Outline:* The rest of the paper is organized as follows. Section II describes the system model and Section III provides the achievable rate analysis. Sum rate maximization problem is investigated in Section V whereas Section IV presents other capacity bounds. In addition, Sections VI and VII study the required fronthaul bit rate and complexity analysis, respectively. Numerical results and discussion are provided in Section VIII, and finally Section IX concludes the paper.

*Notation:* The following notations are adopted in the rest of the paper. Uppercase and lowercase boldface letters are used for matrices and vectors, respectively. The notation  $\mathbb{E}\{\cdot\}$  denotes expectation and  $|\cdot|$  stands for absolute value. The conjugate transpose of vector  $\mathbf{x}$  is defined by  $\mathbf{x}^H$ , and  $\mathbf{X}^T$  denotes the transpose of matrix  $\mathbf{X}$ . In addition,  $x \sim \mathcal{CN}(0, \sigma^2)$  represents a zero-mean circularly symmetric complex Gaussian random variable with variance  $\sigma^2$ . The conjugate of  $x$  is presented as  $x^*$ . Moreover,  $[\mathbf{x}]_n$  denotes the  $n$ th element of  $\mathbf{x}$ .

## II. SYSTEM MODEL

We consider uplink transmission of a cell-free massive MIMO system with  $M$  APs and  $K$  randomly distributed single-antenna users in a large service area. Furthermore, it is assumed that each AP has  $N$  antennas. The channel coefficients between the  $k$ th user and the  $m$ th AP,  $\mathbf{g}_{mk} \in \mathbb{C}^{N \times 1}$ , is modeled as<sup>1</sup>

$$\mathbf{g}_{mk} = \sqrt{\beta_{mk}} \mathbf{h}_{mk}, \quad (1)$$

where  $\beta_{mk}$  denotes the LSF and the elements of  $\mathbf{h}_{mk}$  are independent and identically distributed (i.i.d.)  $\mathcal{CN}(0, 1)$  random variables, representing the SSF [2].<sup>2</sup> The investigation of

<sup>1</sup>A proper channel measurement is necessary to better investigate the channel characteristics of the cell-free massive MIMO and accordingly adjust the resource allocation algorithms [14]. This is left aside for future research.

<sup>2</sup>We assume that the  $K$  LSF coefficients from the  $m$ th AP to the  $K$  users ( $\beta_{mk}, \forall k$ ) are quantized with  $\alpha_m^{\text{LSF}}$  bits resulting in a total number  $K \alpha_m^{\text{LSF}}$  of bits, which need to be sent to the CPU every  $120T_c$ . However, we need to send  $2N(K + \tau_f) \alpha_m^{\text{QF}}$  bits from the  $m$ th AP to the CPU during each  $T_c$  to quantize the received signal and the estimated channel at the  $m$ th AP. Using the fact that  $120 \times 2N(K + \tau_f) \alpha_m^{\text{QF}} \gg K \alpha_m^{\text{LSF}}$ , it is practical to assume that  $\alpha_m^{\text{LSF}}$  is large enough, enabling us to ignore the effect of the quantization distortion.

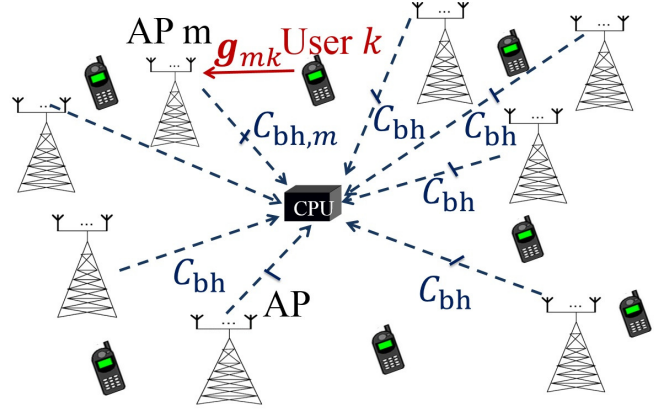


Figure 1. The uplink of a cell-free massive MIMO system with  $K$  single-antenna users and  $M$  APs. Each AP is equipped with  $N$  antennas. The solid lines denote the uplink channels and the dashed lines present the limited capacity fronthaul links between the APs and the CPU.

cell-free massive MIMO with realistic geometry-based channel model [35]–[37] is left for future work.

For each coherence interval, the transmission occurs into 2 main phases: channel estimation and uplink data transmission. In the channel estimation phase, each AP will estimate the channels to all users based on its received pilot signals sent from the users. During the uplink data transmission phase, the users will send the signals to all APs. Then the received signals and the channel estimates at the APs will be quantized and forwarded to the CPU for signal detection. We call this transmission protocol *the QF transmission*. Details of the QF transmission protocol for each coherence interval are as follows.

### A. Uplink Training

All pilot sequences transmitted by all the  $K$  users in the channel estimation phase are collected in a matrix  $\Phi \in \mathbb{C}^{\tau_p \times K}$ , where  $\tau_p$  is the length of the pilot sequence (in symbols) for each user and the  $k$ th column of  $\Phi$ ,  $\phi_k$ , represents the pilot sequence used for the  $k$ th user. After performing a de-spreading operation, the minimum mean square error (MMSE) estimate of the channel coefficient between the  $k$ th user and the  $m$ th AP is given by [2]

$$\hat{\mathbf{g}}_{mk} = c_{mk} \left( \sqrt{\tau_p p_p} \mathbf{g}_{mk} + \sqrt{\tau_p p_p} \sum_{k' \neq k} \mathbf{g}_{mk'} \phi_k^H \phi_{k'} + \mathbf{W}_{p,m} \phi_k \right), \quad (2)$$

where  $\mathbf{W}_{p,m} \in \mathbb{C}^{N \times \tau_p}$  denotes the noise at the  $m$ th AP whose elements are i.i.d.  $\mathcal{CN}(0, 1)$ ,  $p_p$  represents the normalized signal-to-noise ratio (SNR) of each pilot symbol, and  $c_{mk}$  is given by  $c_{mk} = \frac{\sqrt{\tau_p p_p} \beta_{mk}}{\tau_p p_p \sum_{k'=1}^K \beta_{mk'} |\phi_k^H \phi_{k'}|^2 + 1}$ .

### B. Uplink Data Transmission

Let the transmitted signal from the  $k$ th user be  $x_k = \sqrt{q_k} s_k$ , where  $s_k$  ( $\mathbb{E}\{|s_k|^2\} = 1$ ) and  $q_k$  denote the transmitted symbol and the transmit power of the  $k$ th user, respectively. Then the signal received at the  $m$ th AP is given by

$$\mathbf{y}_m = \sqrt{\rho} \sum_{k=1}^K \mathbf{g}_{mk} \sqrt{q_k} s_k + \mathbf{n}_m, \quad (3)$$

Table I. The optimal step size and distortion power of a uniform quantizer with and without the Bussgang decomposition and unit variance input signal [17].

| $\alpha$ | $\Delta_{\text{opt}}$ | $\sigma_{\tilde{n}_d}^2 = \bar{b} - \bar{a}^2 = \sigma_{\tilde{e},B}^2$ | $\bar{a}$ | $\sigma_{\tilde{n}_d}^2 = \sigma_{\tilde{e}}^2$ |
|----------|-----------------------|---|-----------|---|
| 1        | 1.596                 | 0.2313  | 0.6366    | 0.3634 [40]                                     |
| 2        | 0.9957                | 0.10472   | 0.88115   | 0.1188 [40]                                     |
| 3        | 0.586                 | 0.036037  | 0.96256   | 0.03744 [40]                                    |
| 4        | 0.3352                | 0.011409  | 0.98845   | 0.01154 [40]                                    |
| 5        | 0.1881                | 0.003482  | 0.996505  | 0.00349 [40]                                    |
| 6        | 0.1041                | 0.0010389   | 0.99896   | -   |
| 7        | 0.0568                | 0.0003042   | 0.99969   | -   |
| 8        | 0.0307                | 0.0000876   | 0.999912  | -   |

where  $\mathbf{n}_m \in \mathbb{C}^{N \times 1}$ , whose elements are i.i.d.  $CN(0, 1)$ , is the noise at the  $m$ th AP, and  $\rho q_k$  is the normalized uplink SNR corresponding to the  $k$ th user.

### C. Quantization

In this section, we summarize the QF scheme in [17]. With this scheme, first the  $m$ th AP quantizes the estimated channels,  $\hat{\mathbf{g}}_{mk}$ ,  $\forall k$  and the received signal,  $\mathbf{y}_m$ , using the optimal uniform quantization. Then it sends the quantized versions to the CPU. Using the Bussgang decomposition [38], [39], the quantized signal can be expressed as

$$[\check{\mathbf{y}}_m]_n = \tilde{a}[\mathbf{y}_m]_n + [\mathbf{e}_m^{y,B}]_n \quad \forall m, n, \quad (4)$$

where  $\tilde{a}$  is given in Table I and variance of the quantization distortion is given by [17]

$$\sigma_{[\mathbf{e}_m^{y,B}]_n}^2 = \sigma_{\tilde{e},B}^2 \left( \rho \sum_{k'=1}^K \beta_{mk'} q_{k'} + 1 \right), \quad \forall m, n, \quad (5)$$

and it is assumed that the same number of bits is used at all APs and all antennas to quantize the received signal. The optimal values of  $\sigma_{\tilde{e},B}^2$  for different numbers of quantization bits are given in Table I [17], where  $\alpha$  denotes the number of quantization bits. Next, using the analysis in [17], the linear quantization is modeled as  $\mathcal{Q}(z) = h(z) = z + \tilde{n}_d$ ,  $\forall k$ , where the output of the quantizer and the distortion are uncorrelated [40], [41]. Furthermore, the variance of the quantization distortion, is given by

$$\sigma_{\tilde{n}_d}^2 = \begin{cases} \sigma_{\tilde{e}}^2, & \text{obtained in [40],} & \alpha \leq 5, \\ \tilde{a}(1 - \tilde{a}), & [42], & \alpha \geq 6. \end{cases} \quad (6)$$

The resulting  $\sigma_{\tilde{n}_d}^2$  are summarized in Table I. Hence, similar to the scheme in [17], we quantize the estimated channel with the optimal quantizer obtained using the Max algorithm [40] as follows:

$$[\check{\mathbf{g}}_{mk}]_n = [\hat{\mathbf{g}}_{mk}]_n + [\mathbf{e}_{mk}^g]_n, \quad \forall k, n, \quad (7)$$

where the variance of the quantization distortion is

$$\sigma_{[\mathbf{e}_{mk}^g]_n}^2 = \sigma_{[\hat{\mathbf{e}}_{mk}^g]_n}^2 \gamma_{mk} = \sigma_{\tilde{e}g}^2 \gamma_{mk}, \quad \forall m, k, n, \quad (8)$$

where  $\sigma_{\tilde{e}g}^2 = \sigma_{\tilde{e}}^2$ , which is given in Table I, and  $\gamma_{mk} = \sqrt{\tau_p p_p} \beta_{mk} c_{mk}$ .

### D. Data Detection

Let  $\check{\mathbf{V}} \in \mathbb{C}^{MN \times K}$  be the linear detector matrix depending on the side information at the receiver  $\check{\mathbf{g}}_{mk}$ ,  $\forall m, k$ . We assume  $\check{\mathbf{v}}_k = [\check{\mathbf{v}}_{1k}^T, \dots, \check{\mathbf{v}}_{Mk}^T]^T$  refers to the  $k$ th column of the detector matrix  $\check{\mathbf{V}}$ , and  $\check{\mathbf{v}}_{mk} \in \mathbb{C}^N$ . The received signal after using the linear detector at the CPU is given by

$$\check{s}_k = \check{\mathbf{v}}_k^H [\check{\mathbf{y}}_1^T, \dots, \check{\mathbf{y}}_M^T]^T, \quad (9)$$

where  $\check{\mathbf{y}}_m$  is defined in (4). Then the transmitted signals from all  $K$  users will be detected from  $\check{s}_k$ .

## III. ACHIEVABLE RATE ANALYSIS

In this section, we summarize the achievable rate for two common linear receivers, namely ZF and MRC, based on the analysis in [17]. From (4) and (9), the received signal after using the linear detector is

$$\begin{aligned} \check{s}_k &= \sum_{m=1}^M \check{\mathbf{v}}_{mk}^H \check{\mathbf{y}}_m = \sum_{m=1}^M \check{\mathbf{v}}_{mk}^H (\tilde{a} \mathbf{y}_m + \mathbf{e}_m^{y,B}) \\ &= \sum_{m=1}^M \check{\mathbf{v}}_{mk}^H \left( \tilde{a} \sqrt{\rho} \sum_{k=1}^K \hat{\mathbf{g}}_{mk} \sqrt{q_k} s_k + \tilde{a} \mathbf{n}_m + \mathbf{e}_m^{y,B} \right) \\ &= \sum_{m=1}^M \check{\mathbf{v}}_{mk}^H \left( \tilde{a} \sqrt{\rho} \sum_{k=1}^K (\hat{\mathbf{g}}_{mk} - \mathbf{e}_{mk}^g + \check{\mathbf{g}}_{mk}) \sqrt{q_k} s_k + \tilde{a} \mathbf{n}_m + \mathbf{e}_m^{y,B} \right) \\ &= \underbrace{\tilde{a} \sqrt{\rho} q_k \sum_{m=1}^M \check{\mathbf{v}}_{mk}^H \hat{\mathbf{g}}_{mk} s_k}_{\text{DS}_k} + \underbrace{\tilde{a} \sum_{k' \neq k}^K \sqrt{\rho} q_{k'} \sum_{m=1}^M \check{\mathbf{v}}_{mk}^H \hat{\mathbf{g}}_{mk'} s_{k'}}_{\text{IUI}_{kk'}} \\ &\quad + \underbrace{\tilde{a} \sum_{m=1}^M \check{\mathbf{v}}_{mk}^H \mathbf{n}_m}_{\text{TN}_k} + \underbrace{\sum_{m=1}^M \check{\mathbf{v}}_{mk}^H \mathbf{e}_m^{y,B}}_{\text{TQY}_k} - \underbrace{\tilde{a} \sum_{k'=1}^K \sqrt{\rho} \sum_{m=1}^M \check{\mathbf{v}}_{mk}^H \sqrt{q_{k'}} \mathbf{e}_{mk'}^g s_{k'}}_{\text{TQG}_{kk'}} \\ &\quad + \underbrace{\tilde{a} \sum_{k'=1}^K \sqrt{\rho} \sum_{m=1}^M \check{\mathbf{v}}_{mk}^H \sqrt{q_{k'}} \check{\mathbf{g}}_{mk'} s_{k'}}_{\text{TEE}_{kk'}}, \end{aligned} \quad (10)$$

where  $\text{DS}_k$ ,  $\text{IUI}_{kk'}$ , and  $\text{TEE}_{kk'}$  represent the desired signal (DS), interuser interference, and total estimation error (TEE), respectively. Moreover,  $\text{TN}_k$  accounts for the total noise (TN), and finally  $\text{TQY}_k$  and  $\text{TQG}_{kk'}$  are total quantization errors due to quantizing the received signal  $\mathbf{y}_m$  and the estimated channel  $\hat{\mathbf{g}}_{mk}$ , respectively. By using the capacity bound with side information provided in [33], we obtain the following achievable rate

$$R_k^{\text{QF}} \approx \text{ESSF} \left\{ \log_2 \left( 1 + \text{SINR}_k^{\text{QF}} \right) \right\}, \quad (11)$$

where  $\text{SINR}_k^{\text{QF}}$  is defined in (12) (defined at the top of this page), where  $\sigma_{\tilde{e}g}^2 = \sigma_{\tilde{e}}^2$  and  $\sigma_{\tilde{e}y,B}^2 = \sigma_{\tilde{e},B}^2$  while  $\sigma_{\tilde{e}}^2$  and  $\sigma_{\tilde{e},B}^2$  are given in Table I. From (11), we next provide the achievable rates for two common linear decoders: ZF and MRC.

$$\begin{aligned} \text{SINR}_k^{\text{QF}} &= \frac{\mathbb{E} \left\{ |\text{DS}_k s_k | \check{\mathbf{G}}|^2 \right\}}{\sum_{k'=1}^K \mathbb{E} \left\{ |\text{IUI}_{kk'} | \check{\mathbf{G}}|^2 \right\} + \mathbb{E} \left\{ |\text{TN}_k | \check{\mathbf{G}}|^2 \right\} + \frac{1}{\check{a}^2} \mathbb{E} \left\{ |\text{TQY}_k | \check{\mathbf{G}}|^2 \right\} + \sum_{k'=1}^K \mathbb{E} \left\{ |\text{TQG}_{kk'} | \check{\mathbf{G}}|^2 \right\} + \sum_{k'=1}^K \mathbb{E} \left\{ |\text{TEE}_{kk'} | \check{\mathbf{G}}|^2 \right\}}{\rho q_k \left| \sum_{m=1}^M \check{\mathbf{v}}_{mk}^H \check{\mathbf{g}}_{mk} \right|^2}, \quad (12) \\ &= \frac{\rho \sum_{k' \neq k}^K q_{k'} \left| \sum_{m=1}^M \check{\mathbf{v}}_{mk}^H \check{\mathbf{g}}_{mk'} \right|^2 + \rho \sum_{k'=1}^K q_{k'} \sum_{m=1}^M \left[ \beta_{mk'} \left( 1 + \frac{\sigma_{\check{e},B}^2}{\check{a}^2} \right) - \gamma_{mk'} (1 - \sigma_{\check{e}^g}^2) \right] \|\check{\mathbf{v}}_{mk}\|^2 + \left( 1 + \frac{\sigma_{\check{e},B}^2}{\check{a}^2} \right) \sum_{m=1}^M \|\check{\mathbf{v}}_{mk}\|^2}{\rho q_k \left| \sum_{m=1}^M \check{\mathbf{v}}_{mk}^H \check{\mathbf{g}}_{mk} \right|^2}, \quad (14) \end{aligned}$$

$$\text{SINR}_k^{\text{ZF,QF}} = \frac{\rho q_k}{\rho \sum_{k'=1}^K q_{k'} \sum_{m=1}^M \left[ \beta_{mk'} \left( 1 + \frac{\sigma_{\check{e},B}^2}{\check{a}^2} \right) - \gamma_{mk'} (1 - \sigma_{\check{e}^y}^2) \right] \|\check{\mathbf{v}}_{mk}\|^2 + \left( 1 + \frac{\sigma_{\check{e},B}^2}{\check{a}^2} \right) \sum_{m=1}^M \|\check{\mathbf{v}}_{mk}\|^2}. \quad (14)$$

$$\text{SINR}_k^{\text{MRC,QF}} = \frac{\rho q_k \left| \sum_{m=1}^M \check{\mathbf{g}}_{mk}^H \check{\mathbf{g}}_{mk} \right|^2}{\rho \sum_{k' \neq k}^K q_{k'} \left| \sum_{m=1}^M \check{\mathbf{g}}_{mk}^H \check{\mathbf{g}}_{mk'} \right|^2 + \rho \sum_{k'=1}^K q_{k'} \sum_{m=1}^M \left[ \beta_{mk'} \left( 1 + \frac{\sigma_{\check{e},B}^2}{\check{a}^2} \right) - \gamma_{mk'} (1 - \sigma_{\check{e}^y}^2) \right] \|\check{\mathbf{g}}_{mk}\|^2 \left( 1 + \frac{\sigma_{\check{e},B}^2}{\check{a}^2} \right) \sum_{m=1}^M \|\check{\mathbf{g}}_{mk}\|^2}. \quad (16)$$

#### A. Achievable Rate with ZF Receiver

With ZF, the decoder matrix is  $\check{\mathbf{V}} = \check{\mathbf{G}} \left( \check{\mathbf{G}}^H \check{\mathbf{G}} \right)^{-1}$ , where  $\check{\mathbf{G}} = [\check{\mathbf{g}}_1, \dots, \check{\mathbf{g}}_K]$  which yields to

$$\sum_{m=1}^M \check{\mathbf{v}}_{mk}^H \check{\mathbf{g}}_{mk} = \sqrt{\rho q_k},$$

and

$$\sum_{m=1}^M \check{\mathbf{v}}_{mk}^H \check{\mathbf{g}}_{mk'} = 0, \text{ for } k \neq k'.$$

Therefore, the approximate achievable rate for ZF can be simplified as

$$R_k^{\text{ZF,QF}} = \mathbb{E}_{\text{SSF}} \left\{ \log_2 \left( 1 + \text{SINR}_k^{\text{ZF,QF}} \right) \right\}, \quad (13)$$

where  $\mathbb{E}_{\text{SSF}}$  indicates that the expectation is taken over the SSF coefficients, and  $\text{SINR}_k^{\text{ZF,QF}}$  is given by (14) (defined at the top of this page).

#### B. Achievable Rate with MRC Receiver

With MRC, the decoder matrix is  $\check{\mathbf{V}} = \check{\mathbf{G}}$ . Thus, from (11), the achievable rate for MRC can be approximated as

$$R_k^{\text{MRC,QF}} = \mathbb{E}_{\text{SSF}} \left\{ \log_2 \left( 1 + \text{SINR}_k^{\text{MRC,QF}} \right) \right\}, \quad (15)$$

$\text{SINR}_k^{\text{MRC,QF}}$  is given by (16) (defined at the top of the next page).

### IV. OTHER CAPACITY BOUNDS

In this section, for the completeness, we summarize two capacity lower bounds in the literature of cell-free massive MIMO. The first bound is obtained from the UatF bounding technique [33], while the second bound is obtained from another transmission scheme, called the *combine-quantize-and-forward (CQF) scheme*. Compared to the achievable rate in

Section III, these bounds are looser, but can be represented in simple closed-form expressions which depend only on LSF coefficients. As a result, the power control can be performed on the LSF time scale. The comparison of the proposed DL-power control discussed in Section V and the conventional power control using these capacity bounds will help us to evaluate how well the proposed DL-based method works.

#### A. Use-and-then-Forget Capacity Bound

From (10) and by using the UatF bounding technique, we can obtain the following achievable rate

$$R_k^{\text{UatF,QF}} = \log_2 \left( 1 + \text{SINR}_k^{\text{UatF,QF}} \right), \quad (17)$$

where  $R_k^{\text{UatF,QF}}$  is defined in (18) (defined at the top of the next page).

1) *Zero-Forcing Receiver*: As in Section III-A, the ZF decoding matrix is  $\hat{\mathbf{V}} = \hat{\mathbf{G}} \left( \hat{\mathbf{G}}^H \hat{\mathbf{G}} \right)^{-1}$ . Thus, we have  $\text{DS}_k = \sqrt{\rho q_k}$ , and  $\text{Var} \{ \text{DS}_k \} = 0$ . Furthermore we have,

$$\text{IUI}_{kk'} = \rho q_{k'} \sum_{m=1}^M \check{\mathbf{v}}_{mk}^H \check{\mathbf{g}}_{mk'} = 0, \quad (19)$$

$$\begin{aligned} \mathbb{E} \{ |\text{TEE}_{kk'}|^2 \} &= \rho \mathbb{E} \left\{ \left| \sum_{m=1}^M \check{\mathbf{v}}_{mk}^H \sum_{k'=1}^K \sqrt{q_{k'}} \check{\mathbf{g}}_{mk'} \right|^2 \right\} \\ &= \rho \sum_{k'=1}^K q_{k'} \sum_{m=1}^M (\beta_{mk'} - \gamma_{mk'}) \mathbb{E} \{ \|\check{\mathbf{v}}_{mk}\|^2 \}, \quad (20) \end{aligned}$$

$$\mathbb{E} \{ |\text{TN}_k|^2 \} = \mathbb{E} \left\{ \left| \sum_{m=1}^M \check{\mathbf{v}}_{mk}^H \mathbf{n}_m \right|^2 \right\} = \sum_{m=1}^M \mathbb{E} \{ \|\check{\mathbf{v}}_{mk}\|^2 \}, \quad (21)$$

$$\text{SINR}_k^{\text{UatF,QF}} = \frac{|\mathbb{E}\{\text{DS}_k\}|^2}{\text{Var}\{\text{DS}_k\} + \sum_{k' \neq k}^K \mathbb{E}\{|\text{IUI}_{kk'}|^2\} + \sum_{k'=1}^K \mathbb{E}\{|\text{TEE}_{kk'}|^2\} + \sum_{k'=1}^K \mathbb{E}\{|\text{TQG}_{kk'}|^2\} + \frac{1}{\tilde{a}^2} \mathbb{E}\{|\text{TQY}_k|^2\} + \mathbb{E}\{|\text{TN}_k|^2\}}. \quad (18)$$

$$\text{SINR}_k^{\text{ZF,UatF,QF}} = \frac{\rho q_k}{\rho \sum_{k'=1}^K q_{k'} \sum_{m=1}^M \left[ \beta_{mk'} \left( 1 + \frac{\sigma_{\tilde{e},B}^2}{\tilde{a}^2} \right) - \gamma_{mk'} (1 - \sigma_{\tilde{e},B}^2) \right] \mathbb{E}\{|\check{\mathbf{v}}_{mk}|^2\} + \left( 1 + \frac{\sigma_{\tilde{e},B}^2}{\tilde{a}^2} \right) \sum_{m=1}^M \mathbb{E}\{|\check{\mathbf{v}}_{mk}|^2\}}. \quad (25)$$

$$\text{SINR}_k^{\text{MRC,UatF,QF}} = \frac{N^2 q_k \left( \sum_{m=1}^M \gamma_{mk} \right)^2}{N^2 \sum_{k' \neq k}^K q_{k'} \left( \sum_{m=1}^M \gamma_{mk'} \frac{\beta_{mk'}}{\beta_{mk}} \right)^2 |\boldsymbol{\phi}_k^H \boldsymbol{\phi}_{k'}|^2 + N \left( \frac{C_{\text{tot}}}{\tilde{a}^4} + 1 \right) \sum_{m=1}^M \gamma_{mk} \sum_{k'=1}^K q_{k'} \beta_{mk'} + \frac{N}{\rho} \left( \frac{C_{\text{tot}}}{\tilde{a}^4} + 1 \right) \sum_{m=1}^M \gamma_{mk}}. \quad (27)$$

$$\begin{aligned} \mathbb{E}\{|\text{TQY}_k|^2\} &= \mathbb{E}\left\{ \left| \sum_{m=1}^M \check{\mathbf{v}}_{mk}^H \mathbf{e}_m^{y,B} \right|^2 \right\} \\ &= \sum_{m=1}^M \mathbb{E}\{|\check{\mathbf{v}}_{mk}|^2\} \underbrace{\sigma_{\tilde{e},B}^2 \left( \rho \sum_{k'=1}^K \beta_{mk'} q_{k'} + 1 \right)}_{\sigma_{|\mathbf{e}_m^y|,n}^2, \forall n}, \end{aligned} \quad (22)$$

and

$$\begin{aligned} \mathbb{E}\{|\text{TQG}_{kk'}|^2\} &= \rho \mathbb{E}\left\{ \left| \sum_{m=1}^M \check{\mathbf{v}}_{mk}^H \sum_{k'=1}^K \sqrt{q_{k'}} \mathbf{e}_{mk'}^g s_{k'} \right|^2 \right\} \\ &= \rho \sum_{k'=1}^K q_{k'} \sum_{m=1}^M \underbrace{\sigma_{\tilde{e},B}^2 \gamma_{mk'}}_{\sigma_{|\mathbf{e}_{mk'}^g|,n}^2, \forall n} \mathbb{E}\{|\check{\mathbf{v}}_{mk}|^2\}. \end{aligned} \quad (23)$$

Therefore, from (17), the achievable rate of the  $k$ th user for ZF can be simplified as

$$R_k^{\text{ZF,UatF,QF}} = \log_2 \left( 1 + \text{SINR}_k^{\text{ZF,UatF,QF}} \right), \quad (24)$$

where  $\text{SINR}_k^{\text{ZF,UatF,QF}}$  is defined in (25) (given at the top of this page), where  $\mathbb{E}\{|\check{\mathbf{v}}_{mk}|^2\}$  can be numerically calculated.

2) *Maximum-Ratio Combining Receiver*: As in Section III-B, the MRC decoding matrix is  $\hat{\mathbf{V}} = \hat{\mathbf{G}}$ . Thus, from (17), we can obtain an achievable rate for MRC using UatF bounding technique as

$$R_k^{\text{MRC,UatF,QF}} = \log_2 \left( 1 + \text{SINR}_k^{\text{MRC,UatF,QF}} \right), \quad (26)$$

where  $\text{SINR}_k^{\text{MRC,UatF,QF}}$  is given in (27) (defined at the top of this page), where  $C_{\text{tot}} = 2\tilde{a}^2 \sigma_{\tilde{e},B}^2 + \sigma_{\tilde{e},B}^4$ , and note that we use the same number of bits to quantize both signal and channel [15].

The above result is obtained by following the analysis in [15], under the assumption that the Bussgang decomposition is used to quantize both the received signals and the channel estimates.

### B. Achievable Rate of the Combine-Quantize-and-Forward Scheme

The CQF scheme is discussed in [15]. In the CQF scheme, the received signal at the  $m$ th AP, i.e.,  $\mathbf{y}_m$ , is multiplied by the Hermitian of the local channel estimate  $\hat{\mathbf{g}}_{mk}^H$ . The combined signal will be then quantized and forwarded to the CPU. The CPU does not have SSF channel information, so it just uses the statistical properties of the channel (i.e. the LSF) to detect the desired signals. Following the analysis in [15], we obtain the following achievable rate of the  $k$ th user for the CQF scheme

$$R_k^{\text{CQF}} = \log_2 \left( 1 + \text{SINR}_k^{\text{CQF}} \right), \quad (28)$$

where  $\text{SINR}_k^{\text{CQF}}$  is given in (29) (defined at the top of next page), where

$$\boldsymbol{\Gamma}_k = [\gamma_{1k}, \gamma_{2k}, \dots, \gamma_{Mk}]^T, \quad (30a)$$

$$\boldsymbol{\Delta}_{kk'} = \left[ \frac{\gamma_{1k} \beta_{1k'}}{\beta_{1k}}, \frac{\gamma_{2k} \beta_{2k'}}{\beta_{2k}}, \dots, \frac{\gamma_{Mk} \beta_{Mk'}}{\beta_{Mk}} \right]^T, \quad (30b)$$

$$\boldsymbol{\Lambda}_{k'} = \frac{\sigma_{\tilde{e},B}^2}{\tilde{a}^2} \text{diag} \left[ \gamma_{1k'}^2, \dots, \gamma_{Mk'}^2 \right], \quad (30c)$$

$$\mathbf{D}_{kk'} = \left( \frac{\sigma_{\tilde{e},B}^2}{\tilde{a}^2} + 1 \right) \text{diag} \left[ \beta_{1k'} \gamma_{1k}, \dots, \beta_{Mk'} \gamma_{Mk} \right], \quad (30d)$$

$$\mathbf{R}_k = \left( \frac{\sigma_{\tilde{e},B}^2}{\tilde{a}^2} + 1 \right) \text{diag} [\gamma_{1k}, \dots, \gamma_{Mk}], \quad \mathbf{1} = [1, \dots, 1]^T. \quad (30e)$$

## V. SUM RATE MAXIMIZATION PROBLEM

In this section, the sum rate maximization problem is investigated. We show that this is a non-convex problem in its original form, but a simple and heuristic solution can be efficiently solved via GP. For the sake of notation simplicity, the rate of the system is given by

$$R_k = \mathbb{E}_{\text{SSF}} \left\{ \log_2 \left( 1 + \text{SINR}_k \right) \right\}, \quad (31)$$

where the expectation is taken over the SSF coefficients, and  $\text{SINR}_k$  refers to  $\text{SINR}_k^{\text{ZF,QF}}$  and  $\text{SINR}_k^{\text{MRC,QF}}$  for ZF and MRC,

$$\text{SINR}_k^{\text{COF}} = \frac{N^2 \mathbf{1}^T (q_k \mathbf{\Gamma}_k \mathbf{\Gamma}_k^H) \mathbf{1}}{\mathbf{1}^T \left( N^2 \sum_{k' \neq k}^K q_{k'} |\boldsymbol{\phi}_k^H \boldsymbol{\phi}_{k'}|^2 \Delta_{kk'} \Delta_{kk'}^H + N^2 \sum_{k'=1}^K q_{k'} |\boldsymbol{\phi}_k^H \boldsymbol{\phi}_{k'}|^2 \Lambda_{k'} + N \sum_{k'=1}^K q_{k'} \mathbf{D}_{kk'} + \frac{N}{\rho} \mathbf{R}_k \right) \mathbf{1}}, \quad (29)$$

respectively. We aim to choose the transmit power  $q_k, \forall k$ , to maximize the sum rate as follows:

$$P_1 : \max_{q_k} \sum_{k=1}^K \mathbb{E}_{\text{SSF}} \{ \log_2(1 + \text{SINR}_k) \} \quad (32a)$$

$$\text{s.t.} \quad 0 \leq q_k \leq p_{\max}^{(k)}, \forall k, \quad (32b)$$

$$\text{SINR}_k \geq \text{SINR}_k^{\text{Req}}, \forall k. \quad (32c)$$

where  $p_{\max}^{(k)}$  is the maximum transmit power available at the  $k$ th user, and the constraints in (32c) refer to the throughput requirement constraints. Without loss of generality, the optimization Problem  $P_1$  is equivalent to the following problem:

$$P_2 : \max_{q_k} \mathbb{E}_{\text{SSF}} \left\{ \prod_{k=1}^K (1 + \text{SINR}_k) \right\} \quad (33a)$$

$$\text{s.t.} \quad 0 \leq q_k \leq p_{\max}^{(k)}, \forall k, \quad (33b)$$

$$\text{SINR}_k \geq \text{SINR}_k^{\text{Req}}, \forall k. \quad (33c)$$

#### A. Small-Scale-Fading-Based Power Control

To achieve the best performance,  $q_k, \forall k$  should be optimally chosen for each realization inside the expectation. Thus we need to solve the following optimization problem:

$$P_3 : \max_{q_k} \prod_{k=1}^K (1 + \text{SINR}_k) \quad (34a)$$

$$\text{s.t.} \quad 0 \leq q_k \leq p_{\max}^{(k)}, \forall k, \quad (34b)$$

$$\text{SINR}_k \geq \text{SINR}_k^{\text{Req}}, \forall k. \quad (34c)$$

Problem  $P_3$  can be reformulated as follows:

$$P_4 : \min_{q_k} \prod_{k=1}^K (1 + \text{SINR}_k)^{-1} \quad (35a)$$

$$\text{s.t.} \quad 0 \leq q_k \leq p_{\max}^{(k)}, \forall k, \quad (35b)$$

$$\text{SINR}_k \geq \text{SINR}_k^{\text{Req}}, \forall k. \quad (35c)$$

Problem  $P_4$  is a non-convex problem, but it can be reformulated as a standard GP [43]. We re-write Problem  $P_4$  as follows:

$$P_5 : \min_{q_k, t_k} \prod_{k=1}^K (1 + t_k)^{-1} \quad (36a)$$

$$\text{s.t.} \quad 0 \leq q_k \leq p_{\max}^{(k)}, \forall k, \quad (36b)$$

$$\text{SINR}_k \geq t_k, \forall k, \quad (36c)$$

$$\text{SINR}_k \geq \text{SINR}_k^{\text{Req}}, \forall k, \quad (36d)$$

where  $t_k, \forall k$  are the slack variables. Problem  $P_5$  is a non-convex signomial problem. Moreover, all constraints in (36c) and (36d) can be reformulated into posynomial functions. As a result, if the objective function in (36a) is reformulated into a

posynomial function, problem  $P_5$  is a standard GP. Therefore, following the analysis in [44], [45], we present a heuristic solution to tackle the non-convexity issue of Problem  $P_5$ . To end this, we propose to reformulate Problem  $P_6$  as follows:

$$P_6 : \min_{q_k, t_k} \prod_{k=1}^K t_k^{-1} \quad (37a)$$

$$\text{s.t.} \quad 0 \leq q_k \leq p_{\max}^{(k)}, \forall k, \quad (37b)$$

$$\text{SINR}_k \geq t_k, \forall k, \quad (37c)$$

$$\text{SINR}_k \geq \text{SINR}_k^{\text{Req}}, \forall k. \quad (37d)$$

**Proposition 1.** *Problem  $P_6$  can be casted as a standard GP.*

*Proof:* Please refer to Appendix A. ■

**Remark 1.** *We refer the solution obtained by solving Problem  $P_6$  as the SSF-based power control.*

**Remark 2.** *The sum rate optimization power control using the rate formulas (24), (26), and (28) can be solved efficiently by following the same methodology provided in this section.*

**Remark 3.** *We refer to the solution obtained by solving Problem  $P_6$  while using SINR formula obtained by the capacity bounds as the LSF-based power control scheme.*

#### B. Proposed Deep-Learning-Based Power Control

In this section, we first investigate the bottlenecks of the SSF based power control schemes. We present the reasons behind the argument why these schemes are not practically feasible and cannot be implemented in real-time scenarios. Next, we present the proposed DCNN-based power control scheme which relies on only the LSF coefficients. Moreover, the input matrices of the proposed DCNN are provided. Finally, we present the loss function to train the DCNN.

1) *Why are Small-Scale-based Power Control Schemes NOT Practical?:* In the practical systems, some users move very quickly, and hence, the channel coherence time may be only a few milliseconds [27]. Thus, it is not very practical to design the power coefficients based on the SSF. As a result, it is more practical to solve the optimization problem based on only LSF coefficients.

For the SSF-based power control scheme in Section V-A, the optimal transmit powers have to be recomputed on the SSF time scale. It is not practical to re-run the sum rate optimization problem every channel coherence time. The complexity of the sum rate optimization problem makes this approach infeasible. Therefore, we propose to use a deep learning scheme to control the power which needs to be re-run only after many coherence times.

The authors in [32] define the spatial wide-sense stationary (WSS) property which is given by

$$Q_{\text{WSS}} = \frac{T_{\text{LT}}}{T_c}, \quad (38)$$



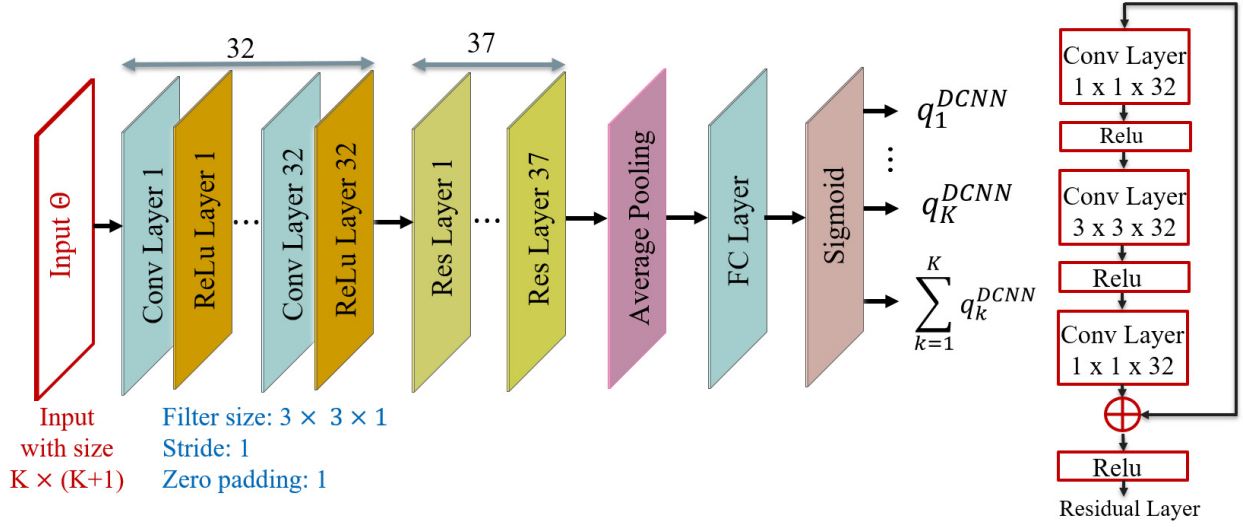


Figure 2. The proposed DL-based power scheme (using DCNN) for cell-free massive MIMO system.

where  $T_{LT}$  refers to the long-term (LT) time, where the statistics of the channel may be considered constant within this interval, whereas  $T_c$  is the channel coherence time. The measurement results for an outdoor scenario at a center frequency of 2 GHz shows that  $Q_{WSS} = 120$ . As a result, the proposed DL-based power needs to be run every  $120T_c$ , while the optimization problem in the channel-based scheme needs to be solved at the beginning of each coherence time.

2) *Deep-Learning-Based Power Control Scheme*: With the proposed scheme, we aim to determine a mapping from the LSF components and the optimal power obtained through solving Problem  $P_5$ , i.e.,  $\mathbf{q}^*$ . To solve this problem we propose a DCNN. The proposed DL-based power control scheme is provided in Figure 2. The SINR in (25) is equivalent to the following SINR formula:

$$\text{SINR}_k^{\text{ZF,UatF,QF,Rewrite}} = \frac{q_k}{\sum_{k'=1}^K q_{k'} A_{kk'} + B_k}, \quad (39)$$

where  $A_{kk'} = \sum_{m=1}^M \left[ \beta_{mk'} \left( 1 + \frac{\sigma_{\epsilon,B}^2}{\bar{a}^2} \right) - \gamma_{mk'} (1 - \sigma_{\epsilon,y}^2) \right] \mathbb{E} \{ \|\check{\mathbf{v}}_{mk}\|^2 \}$  and  $B_k = \frac{1}{\rho} \left( 1 + \frac{\sigma_{\epsilon,y,B}^2}{\bar{a}^2} \right) \sum_{m=1}^M \mathbb{E} \{ \|\check{\mathbf{v}}_{mk}\|^2 \}$ . Next, exploiting (39), we design the input matrix as follows:

$$\Theta_{\text{INPUT}}^{\text{ZF}} = \begin{bmatrix} A_{11} & \dots & A_{1K} & B_1 \\ A_{21} & \dots & A_{2K} & B_2 \\ \vdots & \ddots & \vdots & \vdots \\ A_{K1} & \dots & A_{KK} & B_K \end{bmatrix}. \quad (40)$$

The substitution of  $A_{kk'}$  and  $B_k$  into (40) yields the following input matrix for the case of ZF receiver is given in (41) (defined in the next page). Next, the SINR in (27) is equivalent to the following SINR formula:

$$\text{SINR}_k^{\text{MRC,UatF,QF,Rewrite}} = \frac{q_k}{C_k + \sum_{k'=1}^K q_{k'} D_{kk'} + E_k}, \quad (42)$$

where  $C_k = \frac{\left(\frac{C_{\text{tot}}+1}{\bar{a}^4}\right) \sum_{m=1}^M \gamma_{mk} \beta_{mk}}{N \left(\sum_{m=1}^M \gamma_{m1}\right)^2}$ ,  $D_{kk'} = \frac{\left(\frac{C_{\text{tot}}+1}{\bar{a}^4}\right) \sum_{m=1}^M \gamma_{mk} \beta_{mk'} + N \left(\sum_{m=1}^M \gamma_{mk} \frac{\beta_{mk'}}{\beta_{mk}}\right)^2 |\phi_k^H \phi_{k'}|^2}{N \left(\sum_{m=1}^M \gamma_{mk}\right)^2}$ , and  $E_k = \frac{\left(\frac{C_{\text{tot}}+1}{\bar{a}^4}\right)}{N \rho \sum_{m=1}^M \gamma_{mk}}$ . Next, exploiting (42), we design the input matrix as follows:

$$\Theta_{\text{INPUT}}^{\text{MRC}} = \begin{bmatrix} C_1 & D_{12} & \dots & D_{1K} & E_1 \\ D_{21} & C_2 & \dots & D_{2K} & E_2 \\ \vdots & \ddots & \ddots & \vdots & \vdots \\ D_{K1} & \dots & D_{K(K-1)} & C_K & E_K \end{bmatrix}. \quad (43)$$

The substitution of  $C_k$ ,  $D_{kk'}$  and  $E_k$  into (43) yields the input matrix for the case of MRC receiver is given by (44), defined in the next page. The authors in [27] investigated a multi-cell massive MIMO where the antennas are collocated in the center of the cell, and proposed to use the LSF coefficients as the input of the neural network. This method was shown to work well. However, since the APs in cell-free massive MIMO are distributed, the neural network cannot learn a map between the coefficients  $\beta_{mk}, \forall m, k$  and the power elements obtained by the convex programming software CVX [46] (obtained using the quantized version of the estimated channel).

3) *The Proposed Design for the Case of Non-Active Users*: It is not practical to train the DCNN for all possible system parameters. Let us assume that we train a DCNN for the case of  $K$  users, however only  $K_{\text{serv}}$  ( $K_{\text{serv}} < K$ ) users are active and served in the area. Next, we propose to generate a  $K \times (K+1)$  input matrix with all zeros, except the  $K_{\text{serv}} \times K_{\text{serv}}$  upper left corner and the last  $K_{\text{serv}} \times 1$  column placed in the  $K$ th column of the  $K \times (K+1)$  input matrix. This allows us to exploit the DCNN trained for the case of  $K$  users when we have only  $K_{\text{serv}}$  users in the area. The input matrices for the case of ZF and MRC are given (45) and (46) (defined in the next page).

4) *The Structure of the Proposed DCNN*: As depicted in Fig. 2, the architecture of the proposed neural network consists of five parts: convolution (Conv), residual (Res), average



pooling, fully connected (FC) and sigmoid parts. The input of the network  $\Theta_{\text{INPUT}}$  is a matrix of fixed size  $K \times (K + 1)$ . The input matrix is first passed through the convolution part which consists of a stack of 32 convolution layers. Each convolution layer is followed by the rectified linear unit (ReLU) layer. Each filter in the convolution layer has small receptive field of size  $3 \times 3$  and its stride (i.e., step size of each filter) is fixed to 1 pixel. Furthermore, 1-pixel zero-padding is also carried out in each layer to preserve the spatial resolution after the convolution. Each convolution layer is followed by the ReLU activation layer. The ReLU function introduces non-linearity to the network which helps a variety of complex functions to be learned by training the CNN on a set of training data.

At the next step, the output of the last convolution layer is passed to a stack of 37 residual layers. The basic idea of using these residual layers is based on a state-of-the-art concept in designing neural network architectures [47], called ‘‘shortcut connections’’, that skips one or more layers, as shown in Fig. 2. In practice, the residual learning is often easier to optimize. Each residual layer consists of  $1 \times 1$  and  $3 \times 3$  convolution layers. Each convolution layer is followed by the ReLU activation layer. Then, we skip these convolution layers and add the input directly before the final ReLU activation layer, as depicted in Fig. 2. The stride of  $3 \times 3$  convolution filters in 4-th, 12-th and 34-th residual layers are set to 2 pixels to decrease the spatial resolution step by step. For all convolution filters in other residual layers, the stride is set to 1 pixel and 1-pixel zero-padding is also carried. The output of the last residual layer is then followed by an average pooling layer. We add this layer to aggregate all produced features.

In the FC part, the output of the average pooling layer is fed into one FC layer. The depth of the this FC layer is set to the number of output powers ( $K$ ). Finally, the output of the last FC layer is passed through the sigmoid part to bring the output values in the range  $[0, 1]$ . The output of the network  $\mathbf{q}_{\text{DCNN}}$  is a vector of size  $K$ . In this work, the summation of the uplink power elements is not a fixed value. Therefore, we cannot normalize the output powers as in [27] and [26], where the summation of all output powers are a constant value. In order to force the network to consider this issue, as shown in Fig. 2, we add another output that controls the summation of the predicted powers. We observed that adding this constraint to the network improves the accuracy of the predicted powers. Therefore, the output of the network  $\mathbf{q}_{\text{DCNN}}$  is a vector of size  $K + 1$ .

5) *Training Phase*: For training the above CNN network, first a set containing a large number of training pairs  $(\Theta_{\text{INPUT}}, \mathbf{q}^*)$  are collected, where  $\mathbf{q}^*$  is the solution of Problem  $P_6$ . All inputs are then converted to dB which becomes the input of the network<sup>3</sup>. The above CNN network is trained to minimize the following loss function:

$$L = \|\mathbf{q}^* - \mathbf{q}^{\text{DCNN}}\|^2. \quad (47)$$

This loss is averaged over the training data set and the aim of training is to minimize this loss. The coefficient of weight

<sup>3</sup>Note that the simulation results show that the dB scale provides a better result than the linear scale. Therefore, here we use only the dB scale.

decay is set to 0.0005. Optimization is done by Stochastic Gradient Descent (SGD) using mini-batches of size 512 and the momentum coefficient is 0.9. The initial learning rate is set as 0.001. The learning rate is decreased after 100 epochs by a factor of 100.

## VI. REQUIRED FRONTHAUL BIT RATE

Let us assume the length of the frame (which represents the length of the uplink data) is  $\tau_f = \tau_c - \tau_p$ , where  $\tau_c$  denotes the number of samples for each coherence interval. Defining the number of quantization bits as  $\alpha_m^{\text{QF}}$  and  $\alpha_m^{\text{CQF}}$ , corresponding to the QF and CQF schemes, respectively, where the index  $m$  denotes the  $m$ th AP. For the QF scheme, the required number of bits for each AP to quantize the estimated channel and the uplink data during each coherence interval is  $2\alpha_m^{\text{QF}} \times (NK + N\tau_f)$  whereas we need  $2K\tau_f\alpha_m^{\text{CQF}}$  bits to quantize the signal during each coherence interval for the case of the CQF scheme. Finally  $R_{\text{fh},m}$ , the fronthaul rate of cell-free massive MIMO from the  $m$ th AP to the CPU, is given by

$$R_{\text{fh},m} = \begin{cases} R_{\text{fh},m}^{\text{QF}} = \frac{2N(K + \tau_f)\alpha_m^{\text{QF}}}{T_c}, & \text{QF,} \\ R_{\text{fh},m}^{\text{CQF}} = \frac{2K\tau_f\alpha_m^{\text{CQF}}}{T_c}, & \text{CQF,} \end{cases} \quad (48a)$$

where  $T_c$  (in sec.) refers to the coherence time.

## VII. COMPLEXITY ANALYSIS

Here, we provide the computational complexity analysis for the proposed scheme and the QF and CQF schemes. Note that the MRC receiver has a complexity of  $O(MNK)$  whereas the ZF receiver is designed with the complexity of  $O((M + N)^3)$ . In addition, a standard GP in Problem  $P_7$ , can be solved with complexity equivalent to  $O(K^3)$  [48]. Moreover, note that the optimization problem in the QF scheme needs to be solved at the beginning of each coherence time of the channel whereas the power elements in the proposed LSF-DL-based power control scheme and CQF schemes are obtained at the coherence time of the LSF. Therefore, based on (38), the complexity of solving the optimization problem in QF is  $Q_{\text{WSS}}$  times more than the complexity of the proposed LSF-DL-based power control scheme and the CQF scheme. The number of arithmetic operations are provided in Table II.

## VIII. NUMERICAL RESULTS AND DISCUSSION

In this section, we provide numerical results to validate the performance of the proposed scheme. A cell-free massive MIMO system with  $M$  APs and  $K$  single-antenna users is considered in a  $D \times D$  area, where both APs and users are uniformly distributed at random points. In the following subsections, we define the numerical parameters and then present the corresponding numerical results.

Table II. Computational Complexity of Different Schemes

| Schemes                           | Fronthaul rate                        | Beamforming  | Optimization                   |
|-----------------------------------|---------------------------------------|--------------|--------------------------------|
| MRC, SSF-based QF (Non-practical) | $R_{\text{fh,m}}^{\text{QF}}$ bits/s  | $O(MNK)$     | $Q_{\text{WSS}} \times O(K^3)$ |
| MRC, LSF-DL-based QF              | $R_{\text{fh,m}}^{\text{QF}}$ bits/s  | $O(MNK)$     | $O(K^3)$                       |
| MRC, LSF-based CQF                | $R_{\text{fh,m}}^{\text{CQF}}$ bits/s | $O(MNK)$     | $O(K^3)$                       |
| MRC, LSF-UatF-based QF            | $R_{\text{fh,m}}^{\text{QF}}$ bits/s  | $O(MNK)$     | $O(K^3)$                       |
| ZF, SSF-based QF (Non-practical)  | $R_{\text{fh,m}}^{\text{QF}}$ bits/s  | $O((M+N)^3)$ | $Q_{\text{WSS}} \times O(K^3)$ |
| ZF, LSF-DL-based QF               | $R_{\text{fh,m}}^{\text{QF}}$ bits/s  | $O((M+N)^3)$ | $O(K^3)$                       |
| ZF, LSF-UatF-based QF             | $R_{\text{fh,m}}^{\text{QF}}$ bits/s  | $O((M+N)^3)$ | $O(K^3)$                       |

### A. Simulation Parameters

The channel coefficients between users and APs are modeled in Section 1, where the coefficient  $\beta_{mk}$  is given by  $\beta_{mk} = \text{PL}_{mk} 10^{\frac{\sigma_{sh} z_{mk}}{10}}$ , where  $\text{PL}_{mk}$  is the path loss from the  $k$ th user to the  $m$ th AP and the second term in (1),  $10^{\frac{\sigma_{sh} z_{mk}}{10}}$ , denotes the shadow fading with standard deviation  $\sigma_{sh} = 8$  dB, and  $z_{mk} \sim \mathcal{N}(0, 1)$  [2]. In the simulation, an uncorrelated shadowing model is considered and a three-slope model for the path loss as given in [2]. The noise power is given by  $p_n = \text{BW} \times k_B \times T_0 \times W$ , where  $\text{BW} = 20$  MHz denotes the bandwidth,  $k_B = 1.381 \times 10^{-23}$  represents the Boltzmann constant, and  $T_0 = 290$  (K) denotes the noise temperature. Moreover,  $W = 9$  dB, and denotes the noise figure. It is assumed that  $\bar{p}_p$  and  $\bar{\rho}$  denote the power of the pilot sequence and the uplink data powers, respectively, where  $p_p = \frac{\bar{p}_p}{p_n}$  and  $\rho = \frac{\bar{\rho}}{p_n}$  are normalized transmit SNRs. In simulations, we set  $\bar{p}_p = 100$  mW and  $\bar{\rho} = 1$  W. Similar to [2], we assume that the simulation area is wrapped around at the edges which can simulate an area without boundaries. Hence, the square simulation area has eight neighbors. Moreover, hereafter the term ‘‘orthogonal pilots’’ refers to the case where unique orthogonal pilots are assigned to all users, while in ‘‘random pilot assignment’’ each user is randomly assigned a pilot sequence from a set of orthogonal sequences of length  $\tau_p$  ( $< K$ ), following the approach of [2].

### B. SINR Requirement

To make sure all users can achieve a certain level of throughput, we have  $K$  SINR constraints as indicated in (32c). For the case of ZF receiver, we set

$$\text{SINR}_k^{\text{Req}} = \text{SINR}_k^{\text{ZF,UatF}}(q_k = 1), \forall k. \quad (49)$$

However, for MRC, as indicated in [15], the achievable performance for the cases of the CQF scheme and UatF bounding depends on the system parameters. Therefore, the SINR requirement in this case is defined as follows:

$$\text{SINR}_k^{\text{Req}} = \min \left\{ \text{SINR}_k^{\text{MRC,UatF}}(q_k = 1), \text{SINR}_k^{\text{MRC,Dec}}(q_k = 1) \right\}, \forall k. \quad (50)$$

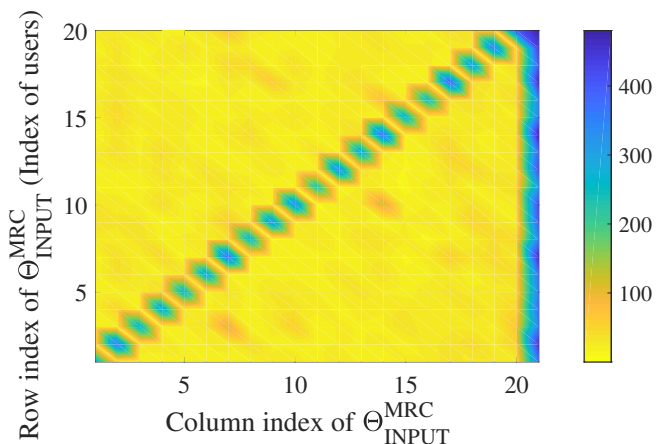


Figure 3. The pattern obtained by taking the average over the LSF coefficients (on a linear scale) for each element of  $\Theta_{\text{INPUT}}^{\text{MRC}}$  for  $M = 15$ ,  $N = 6$ ,  $K = 20$  and  $\tau = 20$ .

### C. How to Generate the Training Set?

For the case of  $M = 15$ ,  $N = 6$ ,  $K = 20$ , we generate 70,000 training sets for both cases of ZF receiver and MRC receiver. To run this simulation setup, we used a PC with Core(TM)i7 CPU @ 3.41 GHz with 64 GB Installed memory (RAM) for 4 days. For the case of  $M = 150$ ,  $N = 1$ ,  $K = 20$ , 60,000 training sets have been produced with the same PC which took 5 days. Moreover, note that training a DCNN takes around 14 hours with this PC. Note that we generate 5,000 samples for the test set.

### D. Pattern in the Input of the Network

In this subsection, we take a closer look at the input of the network and answer the question ‘‘what is the DCNN really doing?’’. To investigate this, we plot the pattern obtained by taking the average over the LSF coefficients for each element of the input matrices  $\Theta_{\text{INPUT}}^{\text{MRC}}$  and  $\Theta_{\text{INPUT}}^{\text{ZF}}$ . Figs. 3 and 4 present the input of DCNN  $\Theta_{\text{INPUT}}^{\text{MRC}}$  for the MRC receiver for  $\{M = 15, N = 6, K = 20\}$  and  $\{M = 150, N = 1, K = 20\}$ , respectively. The size of  $\Theta_{\text{INPUT}}^{\text{MRC}}$  in both cases is  $20 \times 21$  (obtained from (44)). Hence, each row in Figs. 3 and 4

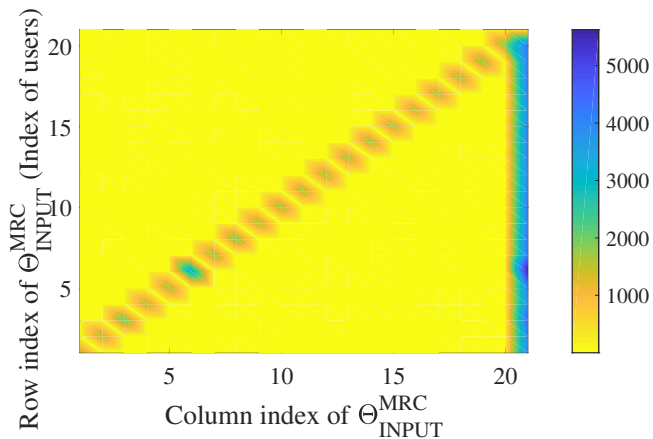


Figure 4. The pattern obtained by taking the average over the LSF coefficients (on a linear scale) for each element of  $\Theta_{\text{INPUT}}^{\text{MRC}}$  for  $M = 150$ ,  $N = 1$ ,  $K = 20$  and  $\tau = 20$ .

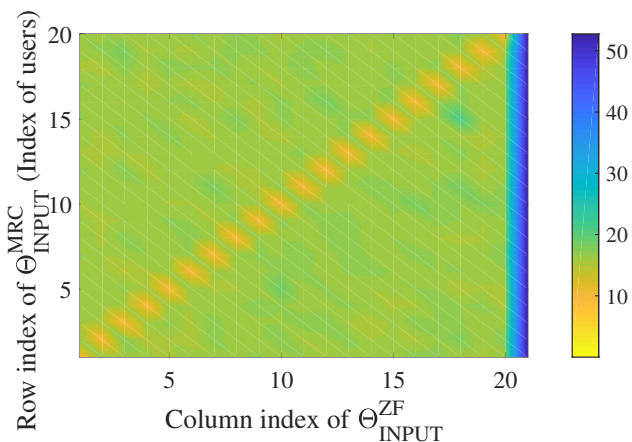


Figure 5. The pattern obtained by taking the average over the LSF coefficients (on a linear scale) for each element of  $\Theta_{\text{INPUT}}^{\text{ZF}}$  for  $M = 15$ ,  $N = 6$ ,  $K = 20$  and  $\tau = 20$ .

indicates the index of the  $k$ th user ( $1 \leq \text{Row index} \leq 20$ ). Ignoring the last column of  $\Theta_{\text{INPUT}}^{\text{MRC}}$ , we have a  $20 \times 20$  matrix, where (based on (44)) the diagonal elements of this matrix are given by  $\frac{(\frac{C_{\text{tot}} + 1}{\alpha^4}) \sum_{m=1}^M \gamma_{mk} \beta_{mk}}{N (\sum_{m=1}^M \gamma_{mk})^2}$  which is referred to as the beamforming gain uncertainty [15]. The last column of the input matrix  $\Theta_{\text{INPUT}}^{\text{MRC}}$  is the total noise power at each user. So, the network tries to find an *unknown map* between the input matrix  $\Theta_{\text{INPUT}}^{\text{MRC}}$  and the optimal power elements obtained by solving the sum rate maximization problem. Next, Fig. 5 presents the pattern obtained by taking the average over the LSF coefficients for each element of the input matrix  $\Theta_{\text{INPUT}}^{\text{ZF}}$ . As a result, the DCNN learns an unknown map between the input matrix  $\Theta_{\text{INPUT}}^{\text{ZF}}$  and the optimal power elements obtained by CVX.

To explain the choice of DCNN intuitively, as our data has a local, spatially invariant structure, it can efficiently be modelled by limiting the connectivity between the successive layers of DNN to local neurons. This significantly reduces the complexity of the network as it is not necessary to allow full connectivity between layers. Moreover, for spatially invariant

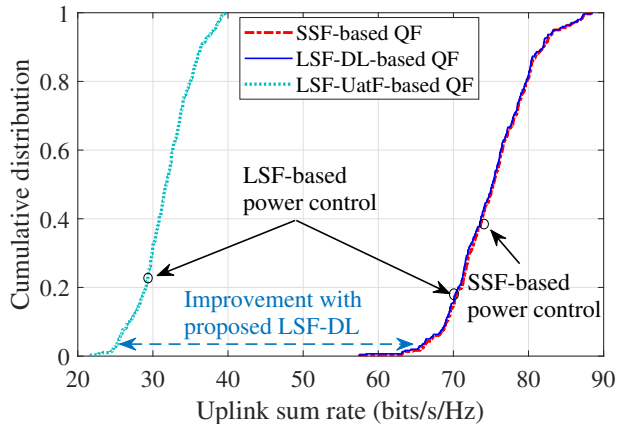


Figure 6. Cumulative distribution of sum rate performance of cell-free massive MIMO with the ZF receiver with  $M = 15$ ,  $K = 20$ ,  $N = 6$ ,  $\tau_p = 20$ ,  $\tau_c = 200$ ,  $\tau_f = \tau_c - \tau_p = 180$  and  $T_c = 1$  ms. Note that we set  $\alpha^{\text{QF}} = 3$  which results in  $R_{\text{th,m}}^{\text{QF}} = \frac{2N(K + \tau_f)\alpha_m^{\text{QF}}}{T_c} = 7.2$  Mbits/s.

data structure the weights between layers also have spatially invariant structure. Thus, the process of excitation of the neurons from one layer to the next can be implemented by a convolution operation. This is computationally very efficient. By neuron output pooling, the spatial dimensionality of the data is gradually reduced from layer to layer, allowing DCNN to model increasingly longer-range correlations between units. Since the DCNN models the spatial correlation among the elements of the input, it needs the input feature space to have a local structure [29]. This enables the DCNN to determine an unknown mapping between the input and the output. However, if there is no local structure in the input, it would be impossible for the DCNN to determine the mapping function between the input and the output (i.e., optimal power elements). As the color maps reveal, there is a strong intensity around the main diagonal elements and also the elements of the last column of the input matrix. The task of the DCNN is to determine an unknown mapping between the input matrix and the output. From the color map, it can be observed that there is a strong correlation, or at least strong interaction, close to the diagonal of the matrix and also close to the elements on the last column of the input matrix. The CNN has the ability to model the correlation among the elements of the input matrix whereas the fully connected network only aggregates the local information learned. This unknown mapping is obtained through modelling the correlation in time and frequency which is done at the DCNN part.

## E. Numerical Results

1) *CDF of the Achievable Sum Rate with ZF*: We evaluate the performance of the proposed uplink sum rate scheme. To assess the performance, a cell-free massive MIMO system is considered with 15 APs ( $M = 15$ ) where each AP is equipped with  $N = 6$  antennas. Moreover, 20 users ( $K = 20$ ) are uniformly distributed at random points over the simulation area of size  $1 \times 1$  km<sup>2</sup>. We also set  $\alpha^{\text{QF}} = 3$  bits resulting



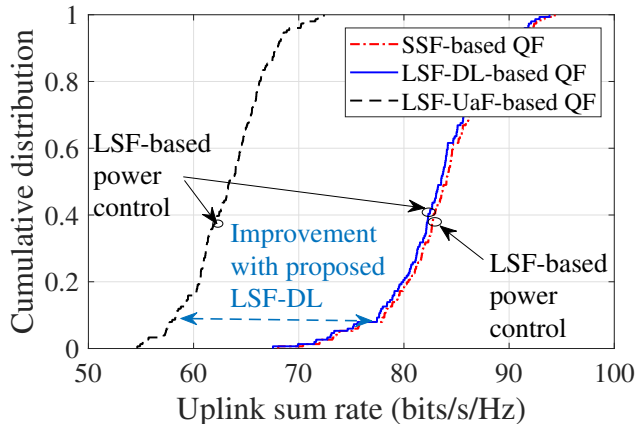


Figure 7. Cumulative distribution of sum rate performance of cell-free massive MIMO with the ZF receiver with  $M = 50$ ,  $K = 20$ ,  $N = 2$ ,  $\tau_p = 20$ ,  $\tau_c = 200$ ,  $\tau_f = \tau_c - \tau_p = 180$  and  $T_c = 1$  ms. Note that we set  $\alpha^{\text{QF}} = 3$  which results in  $R_{\text{th,m}}^{\text{QF}} = \frac{2N(K+\tau_f)\alpha_m^{\text{QF}}}{T_c} = 1.8$  Mbits/s.

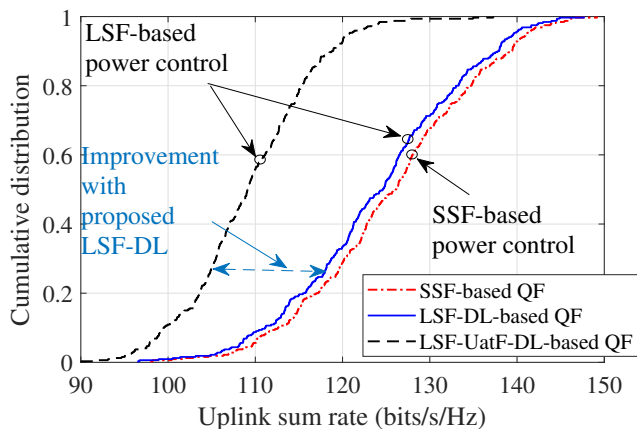


Figure 8. Cumulative distribution of sum rate performance of cell-free massive MIMO with the ZF receiver with  $M = 50$ ,  $K = 20$ ,  $N = 2$ ,  $\tau_p = 20$  and with perfect and error-free fronthaul links.

in

$$R_{\text{th,m}}^{\text{QF}} = \frac{2N(K+\tau_f)\alpha_m^{\text{QF}}}{T_c} = 7.2 \text{ Mbits/s.} \quad (51)$$

Fig. 6 presents the cumulative distribution of the achievable uplink sum rates with the ZF receiver for the proposed LSF-DL-based power scheme, the UaF bounding technique and the QF scheme (where the power elements are designed based on the quantized version of the estimated channel). As seen in Fig. 6, the performance of the proposed LSF-DL-based power scheme is significantly improved compared to the performance of the UaF bounding scheme. Moreover, note that in Fig. 6, the power elements in “the quantized channel” are designed based on the quantized version of the channel whereas in “LSF-DL-based QF”, we need only the statistics of the channel to solve the optimization problems. Note that, in “LSF-UaF-based QF”, the CPU has access to the quantized version of the estimated channel to detect the data, however, it exploits only LSF coefficients to design the power elements. Note that it is practically impossible to design the power elements based on

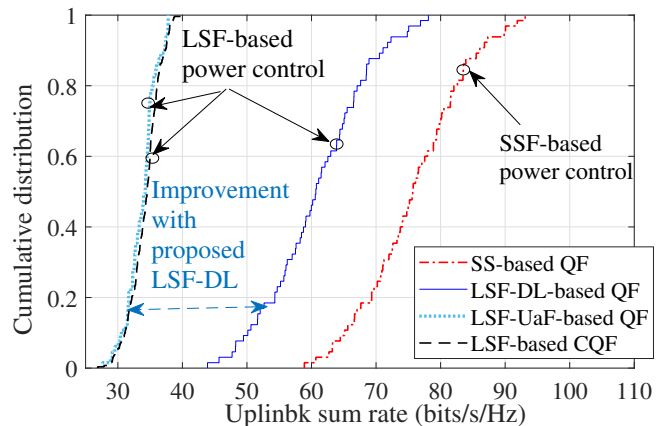


Figure 9. Cumulative distribution of sum rate performance of cell-free massive MIMO with the MRC receiver with  $M = 150$ ,  $K = 20$ ,  $N = 1$ ,  $\tau_p = 15$  and perfect and error-free fronthaul links.

the quantized version of the channel due to its high complexity. It is very interesting that the sum rate performance of cell-free massive MIMO with the power elements obtained from the quantized version of the channel is almost as good as the performance of cell-free massive MIMO with the power elements obtained from the quantized version of the estimated channel -which reveals the beauty of DCNN.

Next, we investigate the performance of cell-free massive MIMO with the ZF receiver for  $M = 50$  APs, each equipped with  $N = 2$  antennas,  $K = 20$  users, and  $\alpha^{\text{QF}} = 3$  bits. Fig. 7 presents the cumulative distribution of sum rate performance of the cell-free massive MIMO system with three schemes, i.e., the UaF bounding technique, the proposed LSF-DL power control scheme and the scheme in which quantized version of the estimated channel are exploited to solve the sum rate maximization problem.

In Fig. 8, we investigate the performance of the cell-free massive MIMO with  $M = 50$ ,  $N = 2$ , and  $K = 20$  and perfect and error-free fronthaul links. We can see that the performance of the proposed LSF-DL-based power scheme is significantly enhanced compared to the performance of the UaF bounding scheme. Finally, in Fig. 9, we consider a cell-free massive MIMO system with  $M = 150$ ,  $N = 1$ , and  $K = 20$  and perfect and error-free fronthaul links. The figure confirms the significant improvement achieved by the proposed LSF-DL-based power scheme. Moreover, note that reference [34] considers the MRC receiver and with only the case that the APs combine the received signals by multiplying them with the conjugate of the channel estimates, which is equivalent to the CQF scheme with error-free fronthaul links (the dashed black line in Fig. 9). As a result, the performance of [34] cannot be better than the dashed black line in Fig. 9.

2) *CDF of the Achievable Sum Rate with MRC*: Next, we consider the cell-free massive MIMO with the MRC receiver and with  $M = 15$  APs,  $N = 6$  antennas per-AP and  $K = 20$  users uniformly distributed over the area. Moreover, we set

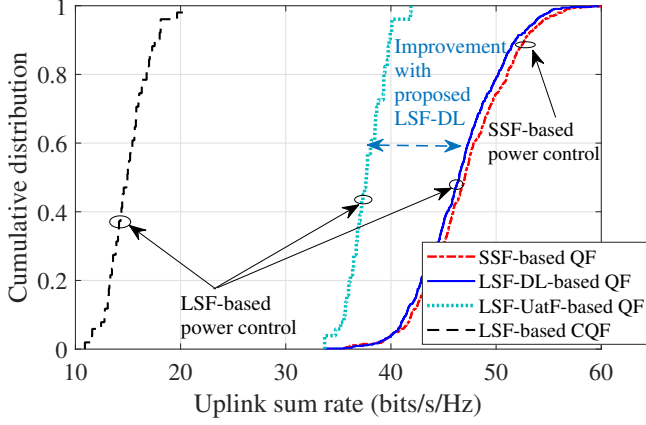


Figure 10. Cumulative distribution of sum rate performance of cell-free massive MIMO with the MRC receiver with  $M = 15$ ,  $K = 20$ ,  $N = 6$ ,  $\tau_p = 20$ ,  $\tau_c = 200$ ,  $\tau_f = \tau_c - \tau_p = 180$  and  $T_c = 1$  ms. Note that we set  $\alpha^{\text{QF}} = 3$  and  $\alpha^{\text{CQF}} = 1$  which results in  $R_{\text{fh,m}}^{\text{QF}} = \frac{2N(K+\tau_f)\alpha_m^{\text{QF}}}{T_c} = 7.2$

$$\text{Mbits/s } R_{\text{fh}}^{\text{CQF}} = \frac{2K\tau_f\alpha_m^{\text{CQF}}}{T_c} = 7.2 \text{ Mbits/s.}$$

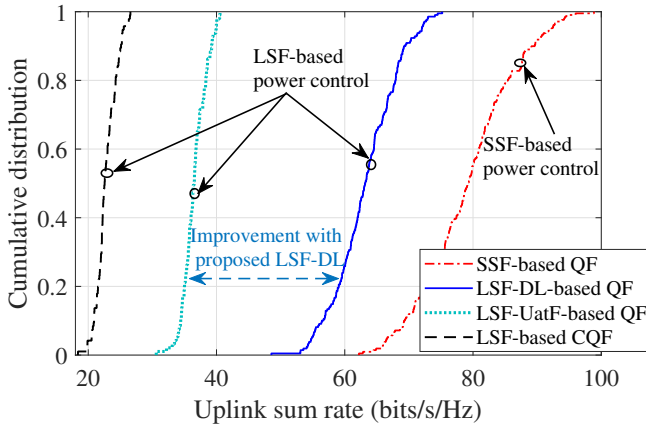


Figure 11. Cumulative distribution of sum rate performance of cell-free massive MIMO with the MRC receiver with  $M = 150$ ,  $K = 20$ ,  $N = 1$ ,  $\tau_p = 20$ ,  $\tau_c = 200$ ,  $\tau_f = \tau_c - \tau_p = 180$  and  $T_c = 1$  ms. Note that we set  $\alpha^{\text{QF}} = 18$  and  $\alpha^{\text{CQF}} = 1$  which results in  $R_{\text{fh,m}}^{\text{QF}} = \frac{2N(K+\tau_f)\alpha_m^{\text{QF}}}{T_c} = 7.2$

$$\text{Mbits/s } R_{\text{fh}}^{\text{CQF}} = \frac{2K\tau_f\alpha_m^{\text{CQF}}}{T_c} = 7.2 \text{ Mbits/s.}$$

$\alpha^{\text{QF}} = 3$  and  $\alpha^{\text{CQF}} = 1$  resulting in

$$R_{\text{fh,m}}^{\text{QF}} \left( = \frac{2N(K+\tau_f)\alpha_m^{\text{QF}}}{T_c} \right) = R_{\text{fh,m}}^{\text{CQF}} \left( = \frac{2K\tau_f\alpha_m^{\text{CQF}}}{T_c} \right) = 7.2 \text{ Mbits/s.} \quad (52)$$

Hence, the required fronthaul rate is the same in all schemes. Fig. 10 shows the cumulative distribution of the achievable uplink sum rates for the proposed LSF-DL-based power scheme, the UaF bounding technique, the CQF scheme and the QF schemes. As seen in Fig. 10, the performance of the proposed LSF-DL-based power scheme is significantly improved compared to the performance of CQF scheme and the UaF bounding scheme.

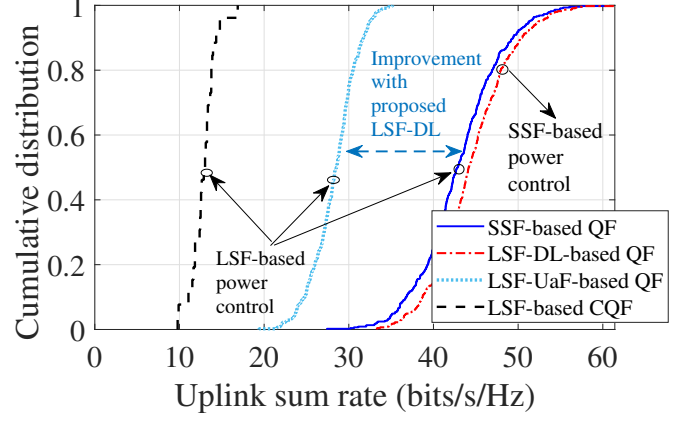


Figure 12. Cumulative distribution of sum rate performance of cell-free massive MIMO with the MRC receiver with  $M = 15$ ,  $K = 20$ ,  $N = 6$ ,  $\tau_p = 15$ ,  $\tau_c = 200$ ,  $\tau_f = \tau_c - \tau_p = 185$  and  $T_c = 1$  ms. Note that we set  $\alpha^{\text{QF}} = 3$  and  $\alpha^{\text{CQF}} = 1$  which results in  $R_{\text{fh,m}}^{\text{QF}} = \frac{2N(K+\tau_f)\alpha_m^{\text{QF}}}{T_c} = 7.38$

$$\text{Mbits/s } R_{\text{fh}}^{\text{CQF}} = \frac{2K\tau_f\alpha_m^{\text{CQF}}}{T_c} = 7.4 \text{ Mbits/s.}$$

Next, to further investigation on the system performance, in Fig. 11, we present the cumulative distribution of sum rate performance of the cell-free massive MIMO system with the MRC receiver and  $M = 150$ ,  $N = 1$ ,  $K = 20$ ,  $\tau_p = 20$ ,  $T_c = 1$  ms, and  $\alpha^{\text{QF}} = 18$  bits (which again results in 7.2 Mbits/s fronthaul rate). The figure shows that the performance of the cell-free massive MIMO system significantly improves using the proposed LSF-DL based power control compared to the UaF bounding technique and the CQF scheme while in all schemes we exploit the same amount of fronthaul rate (i.e., 7.2 Mbits/s), and the power elements are designed based on the LSF coefficients in all the UaF bounding technique, the CQF scheme and the proposed LSF-based scheme. Moreover, as expected the case when the quantized version of the estimated channel is exploited to design the power coefficients provides the best performance. A cell-free massive MIMO is considered with  $M = 15$  APs and  $K = 20$  users. Moreover,  $\tau_p = 15$  pilot sequences are randomly assigned to the users. Moreover, we set  $\alpha^{\text{QF}} = 3$  and  $\alpha^{\text{CQF}} = 1$ . Fig. 12 presents the cumulative distribution of the achievable uplink sum rates of the system where the input matrix  $\Theta_{\text{INPUT}}^{\text{MRC}}$ , given in (44), is exploited to model the non-orthogonal pilot sequences. As the figure shows, the proposed LSF-DL-based power scheme substantially increases the performance of the system compared to the other LSF-based schemes.

The results in Figs. 6- 12 show that the proposed LSF-DL-based power control scheme provides a better performance if we have multiple antennas per AP. This is because a larger number of antennas per AP improves the channel hardening [9], resulting in a tighter UaF SINR bound. Note that the input matrix of the DCNN is designed based on the SINR obtained by the UaF bounding technique.

3) *A Close Look at the Output of DCNN*: Next, assuming the system set-up in the previous subsection, we take a closer look at the output of the neural network. Fig. 13 presents a comparison between the optimal power elements obtained

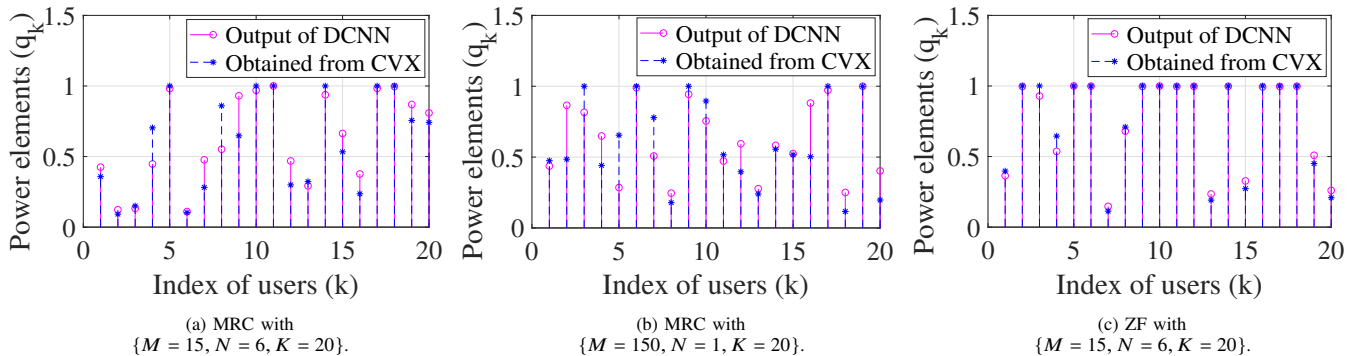
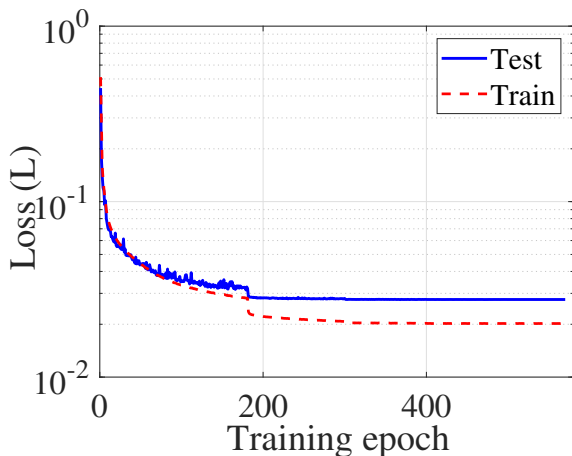
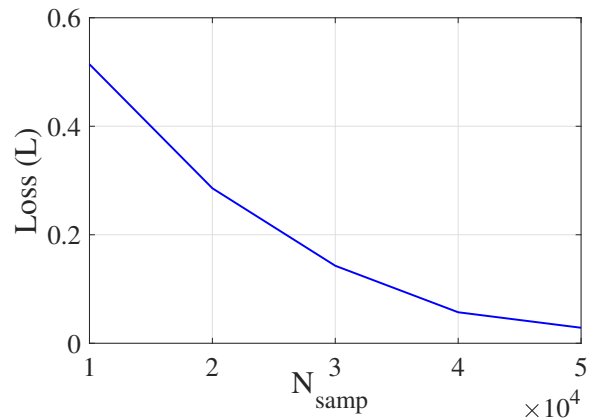


Figure 13. The power elements obtained by solving the sum rate maximization problem by CVX based on the quantized version of the estimated channel versus the power elements obtained by a trained DCNN with only LSF components.



(a) Loss function for both training and test sets.



(b) The error bound.

Figure 14. The training curve for ZF receiver with  $M = 15$ ,  $N = 6$ , and  $K = 20$

by solving the sum rate maximization Problem  $P_6$  (using the quantized channel to solve the sum rate maximization problem) and the power elements obtained by the trained DCNN. The dashed (blue) lines in Figs. 13a (for the MRC receiver and with  $\{M = 15, N = 6, K = 20\}$ ), 13b (for the MRC receiver and with  $\{M = 150, N = 6, K = 20\}$ ) and 13c (for the ZF receiver and with  $\{M = 15, N = 6, K = 20\}$ ) show the optimal power elements to maximize the sum rate performance of the system, obtained by CVX (which are designed based on the quantized version of the estimated instantaneous channel. Moreover, the solid (magenta) lines indicate the power elements obtained by the trained network. Note that the difference between the power elements obtained by CVX and the power elements obtained by the DCNN is due to lack of the information about the quantized version of the estimated instantaneous channel at the input of the DCNN. Hence, it is not possible to achieve the exact power elements obtained by CVX from knowledge of the LSF coefficients as the input of the DCNN.

#### F. Training Curve

Fig. 14a demonstrates the loss function for both training and test sets, which shows less than 0.02% loss (see (47)), confirming the accuracy of the proposed training scheme. Note

that it is impossible to achieve the exact performance of the QF scheme with only the statistics of the channel (as the CPU exploits knowledge of the quantized version of the estimated channel to design the power elements).

Next, we investigate the error bound and the effect of the number of training samples, i.e.,  $N_{\text{samp}}$ , on the performance of the loss function. To investigate this, we plot the loss function versus total number of training samples for the case of the ZF receiver with  $\{M = 15, N = 6, K = 20\}$  in Fig. 14b. As the figure shows the loss decreases as the total number of training sets,  $N_{\text{samp}}$ , increases.

#### G. Is It Possible to Use the Same DCNN When a Number of Users Are Inactive?

We investigate the performance of cell-free massive MIMO with the ZF receiver for  $M = 50$  APs, each equipped with  $N = 2$  antennas, and  $K_{\text{serv}} = 5$  users while using the DCNN trained for  $K = 20$  users, as assumed in Fig. 7. We design the input matrix as described in (45) with  $K = 20$  and  $K_{\text{serv}} = 5$ . Fig. 15 presents the cumulative distribution of the sum rate performance of the system with three schemes, i.e., the UatF bounding technique, the proposed LSF-DL power control scheme and the scheme in which the quantized version of the estimated channel is exploited to solve the sum rate



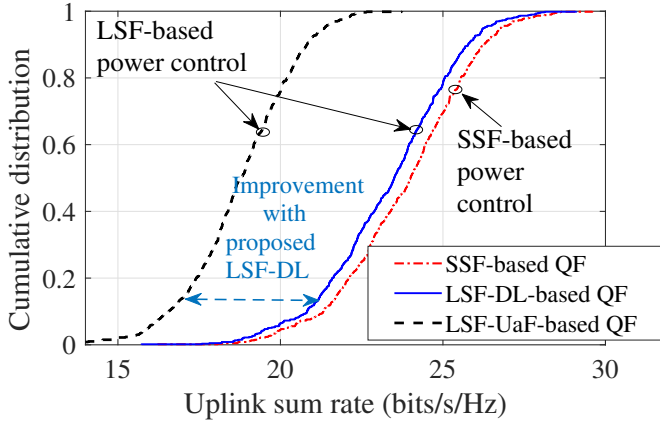


Figure 15. Cumulative distribution of sum rate performance of cell-free massive MIMO with the ZF receiver with  $M = 50$ ,  $K_{\text{serv}} = 5$ ,  $N = 2$ ,  $\tau_p = 5$ ,  $\tau_c = 200$ ,  $\tau_f = \tau_c - \tau_p = 195$  and  $T_c = 1$  ms. Note that we set  $\alpha^{\text{QF}} = 3$  which results in  $R_{\text{th},m}^{\text{QF}} = \frac{2N(K+\tau_f)\alpha_m^{\text{QF}}}{T_c} = 1.8$  Mbits/s. We use the DCNN trained for the case of  $K = 20$  users when we have only  $K_{\text{serv}} = 5$  active users in the area.

maximization problem. As the figure shows, the proposed scheme works very well even if we have fewer active users in the area. This shows that the proposed DCNN scheme is very practical and it is enough to train the network only once, for a large number of users, and use this DCNN for all the cases when a smaller number of users are active in the simulation area.

## IX. CONCLUSIONS

We have considered limited-fronthaul cell-free massive MIMO, and a performance comparison between two ways of the implementing cell-free massive MIMO uplink, namely, the QF scheme (for the ZF and MRC receiver) and CQF scheme (for the MRC receiver) have been presented. The sum rate maximization problem has been formulated considering the per-use power constraints and the SINR requirement constraints, and taking account the quantization distortions. Next, we have developed a deep learning algorithm using a neural network to find a mapping between the LSF components and the power elements obtained from the SSF coefficient. We have proposed a sum rate optimization scheme with LSF-DL-based power control, which is practically feasible in cell-free massive MIMO due to its low complexity. We have shown that our data has a local structure for which DCNN is particularly suited. The results show less than 0.02% loss. We have studied the pattern in the input of the deep learning network and presented the error bound. The numerical results show that the proposed LSF-DL-based power control scheme increases the median of the cumulative distribution of the achievable uplink sum rate of the cell-free massive MIMO system by more than three times (depending on the system parameters), compared to the existing practical schemes. Finally, we have presented a novel design to adopt the proposed DCNN for the case when some users are not active.

## APPENDIX A: PROOF OF PROPOSITION 1

The standard form of GP is defined as follows [49]:

$$P_{\text{GP}} : \min f_0(\mathbf{x}), \quad (53a)$$

$$\text{s.t. } f_i(\mathbf{x}) \leq 1, i = 1, \dots, m, g_i(\mathbf{x}) = 1, i = 1, \dots, p, \quad (53b)$$

where  $f_0$  and  $f_i$  are posynomial and  $g_i$  are monomial. Moreover,  $\mathbf{x} = \{x_1, \dots, x_n\}$  contains the optimization variables. First, we consider the ZF receiver, where the SINR is given in (14) while the optimization problem is solved using the quantized version of the estimated instantaneous channel. Using (14), the SINR constraint in (37c) is not a posynomial function in its initial form, however it can be rewritten as the posynomial function, given in (54), defined at the top of the next page. By applying a simple transformation, (54) is equivalent to the following inequality:

$$q_k^{-1} \left( \sum_{k'=1}^K v_{kk'} q_{k'} + w_k \right) \leq \frac{1}{t}, \quad (55)$$

where

$$v_{kk'} = \sum_{m=1}^M \left[ \beta_{mk'} \left( 1 + \frac{\sigma_{\bar{e},B}^2}{\bar{a}^2} \right) - \gamma_{mk'} (1 - \sigma_{\bar{e},B}^2) \right] \|\check{\mathbf{v}}_{mk}\|^2, \quad (56)$$

and

$$w_k = \frac{1}{\rho} \left( 1 + \frac{\sigma_{\bar{e},B}^2}{\bar{a}^2} \right) \sum_{m=1}^M \|\check{\mathbf{v}}_{mk}\|^2. \quad (57)$$

The transformation in (55) shows that the left-hand side of (54) is a posynomial function. Moreover, the SINR constraint in (37d) is not a posynomial function in its original form, however, through some mathematical manipulation, it can be written as given in (58), defined at the top of the next page. By applying a simple transformation, (37d) is equivalent to the following inequality:

$$q_k^{-1} \left( \sum_{k'=1}^K v_{kk'} q_{k'} + w_k \right) \leq \frac{1}{\text{SINR}_k^{\text{Req}}}. \quad (59)$$

Therefore, the power allocation Problem  $P_6$  is a standard GP (convex problem), where the objective function and constraints are monomial and posynomial. Next, we consider the MRC receiver. The SINR constraint in (35c) is not a posynomial function, however by applying a simple transformation, it can be shown that using the SINR formulas in (16), the SINR constraints in (37c) and (37d) can be written in the following forms:

$$q_k^{-1} \left( \sum_{k' \neq k}^K a_{kk'} q_{k'} + \sum_{k'=1}^K b_{kk'} q_{k'} + c_k \right) \leq \frac{1}{t}, \quad (60)$$

and

$$q_k^{-1} \left( \sum_{k' \neq k}^K a_{kk'} q_{k'} + \sum_{k'=1}^K b_{kk'} q_{k'} + c_k \right) \leq \frac{1}{\text{SINR}_k^{\text{Req}}}, \quad (61)$$

where

$$a_{kk'} = \frac{\left| \sum_{m=1}^M \check{\mathbf{g}}_{mk}^H \check{\mathbf{g}}_{mk'} \right|^2}{\left| \sum_{m=1}^M \check{\mathbf{g}}_{mk}^H \check{\mathbf{g}}_{mk} \right|^2}, \quad (62)$$

$$\frac{\rho \sum_{k'=1}^K q_{k'} \sum_{m=1}^M \left[ \beta_{mk'} \left( 1 + \frac{\sigma_{\tilde{e},B}^2}{\tilde{a}^2} \right) - \gamma_{mk'} (1 - \sigma_{\tilde{e},y}^2) \right] \|\check{\mathbf{v}}_{mk}\|^2 + \left( 1 + \frac{\sigma_{\tilde{e},y,B}^2}{\tilde{a}^2} \right) \sum_{m=1}^M \|\check{\mathbf{v}}_{mk}\|^2}{\rho q_k} \leq \frac{1}{t}, \forall k. \quad (54)$$

$$\frac{\rho \sum_{k'=1}^K q_{k'} \sum_{m=1}^M \left[ \beta_{mk'} \left( 1 + \frac{\sigma_{\tilde{e},B}^2}{\tilde{a}^2} \right) - \gamma_{mk'} (1 - \sigma_{\tilde{e},y}^2) \right] \|\check{\mathbf{v}}_{mk}\|^2 + \left( 1 + \frac{\sigma_{\tilde{e},y,B}^2}{\tilde{a}^2} \right) \sum_{m=1}^M \|\check{\mathbf{v}}_{mk}\|^2}{\mathbf{u}_k^H (N^2 q_k \mathbf{\Gamma}_k \mathbf{\Gamma}_k^H) \mathbf{u}_k} \leq \frac{1}{\text{SINR}_k^{\text{Req}}}, \forall k. \quad (58)$$

$$b_{kk'} = \frac{\sum_{m=1}^M \left[ \beta_{mk'} \left( 1 + \frac{\sigma_{\tilde{e},B}^2}{\tilde{a}^2} \right) - \gamma_{mk'} (1 - \sigma_{\tilde{e},y}^2) \right] \|\check{\mathbf{g}}_{mk}\|^2}{\left| \sum_{m=1}^M \check{\mathbf{g}}_{mk}^H \check{\mathbf{g}}_{mk} \right|^2}, \quad (63)$$

and

$$c_k = \frac{\mathbf{u}_k^H \mathbf{R}_k \mathbf{u}_k}{\rho \left( 1 + \frac{\sigma_{\tilde{e},y,B}^2}{\tilde{a}^2} \right) \sum_{m=1}^M \|\check{\mathbf{g}}_{mk}\|^2}. \quad (64)$$

This completes the proof of Proposition 1.  $\blacksquare$

## REFERENCES

- [1] M. Bashar, A. A. K. Cumanan, H. Q. Ngo, A. G. Burr, and P. X. M. Debbah, "Deep learning-aided finite-capacity fronthaul cell-free massive MIMO with zero forcing," in *Proc. IEEE ICC*, Jun. 2020, pp. 1–6.
- [2] H. Q. Ngo, A. Ashikhmin, H. Yang, E. G. Larsson, and T. L. Marzetta, "Cell-free massive MIMO versus small cells," *IEEE Trans. Wireless Commun.*, vol. 16, no. 3, pp. 1834–1850, Mar. 2017.
- [3] E. Nayebi, A. Ashikhmin, T. L. Marzetta, H. Yang, and B. D. Rao, "Precoding and power optimization in cell-free massive MIMO systems," *IEEE Trans. Wireless Commun.*, vol. 16, no. 7, pp. 4445–4459, Jul. 2017.
- [4] M. Bashar, K. Cumanan, A. G. Burr, M. Debbah, and H. Q. Ngo, "On the uplink max-min SINR of cell-free massive MIMO systems," *IEEE Trans. Wireless Commun.*, vol. 18, no. 24, pp. 2021–2036, Jan. 2019.
- [5] M. Bashar, K. Cumanan, A. G. Burr, H. Q. Ngo, L. Hanzo, and P. Xiao, "On the performance of cell-free massive MIMO relying on adaptive NOMA/OMA mode-switching," *IEEE Trans. Commun.*, vol. 68, no. 2, pp. 792–810, Feb. 2020.
- [6] M. Bashar, *Cell-free massive MIMO and Millimeter Wave Channel Modelling for 5G and Beyond*. Ph.D. dissertation, University of York, United Kingdom, 2019.
- [7] S. Buzzi and C. D'Andrea, "Cell-free massive MIMO: user-centric approach," *IEEE Wireless Commun. Lett.*, vol. 6, no. 6, pp. 1–4, Aug. 2017.
- [8] J. Zhang, Y. Wei, E. Björnson, Y. Han, and S. Jin, "Performance analysis and power control of cell-free massive MIMO systems with hardware impairments," *IEEE Access*, vol. 6, pp. 55 302–55 314, Sep. 2018.
- [9] Z. Chen and E. Björnson, "Channel hardening and favorable propagation in cell-free massive MIMO with stochastic geometry," *IEEE Trans. Commun.*, vol. 66, no. 11, pp. 5205–5219, Nov. 2018.
- [10] E. Nayebi, A. Ashikhmin, T. L. Marzetta, and B. D. Rao, "Performance of cell-free massive MIMO systems with MMSE and LSFD receivers," in *IEEE Asilomar*, Nov. 2016.
- [11] M. Sarajlić, F. Rusek, J. Rodríguez Sánchez, L. Liu, and O. Edfors, "Fully decentralized approximate zero-forcing precoding for massive MIMO systems," *IEEE Wireless Commun. Lett.*, vol. 8, no. 3, pp. 773–776, Jun. 2019.
- [12] C. Jeon, K. Li, J. R. Cavallaro, and C. Studer, "Decentralized equalization with feedforward architectures for massive MU-MIMO," *IEEE Trans. Signal Process.*, vol. 67, no. 17, pp. 4418–4432, Sep. 2019.
- [13] M. Bashar, K. Cumanan, A. G. Burr, M. Debbah, and H. Q. Ngo, "Enhanced max-min SINR for uplink cell-free massive MIMO systems," in *Proc. IEEE ICC*, May 2018, pp. 1–6.
- [14] G. Interdonato, E. Björnson, H. Q. Ngo, P. Frenger, and E. G. Larsson, "Ubiquitous cell-free massive MIMO communications," *EURASIP J. Wireless Commun. Netw.*, pp. 1–19, To appear.
- [15] M. Bashar, K. Cumanan, A. G. Burr, H. Q. Ngo, and M. Debbah, "Max-min SINR of cell-free massive MIMO uplink with optimal uniform quantization," *IEEE Trans. Commun.*, To appear.
- [16] A. G. Burr, M. Bashar, and D. Maryopi, "Cooperative access networks: Optimum fronthaul quantization in distributed massive MIMO and cloud RAN," in *Proc. IEEE VTC*, Jun. 2018, pp. 1–7.
- [17] M. Bashar, H. Q. Ngo, A. Burr, D. Maryopi, K. Cumanan, and E. G. Larsson, "On the performance of backhaul constrained cell-free massive MIMO with linear receivers," in *Proc. IEEE Asilomar*, Nov. 2018, pp. 1–7.
- [18] A. G. Burr, M. Bashar, and D. Maryopi, "Ultra-dense radio access networks for smart cities: Cloud-RAN, Fog-RAN and cell-free massive MIMO," in *Proc. IEEE PIMRC*, Sep. 2018, pp. 1–5.
- [19] *Common Public Radio Interface (CPRI)*. Interface Specification V6.0, Aug 2013.
- [20] T. Rep, *C-RAN: the road towards green RAN*. China Mobile Research Institute, Oct 2011.
- [21] M. Bashar, K. Cumanan, A. G. Burr, H. Q. Ngo, and M. Debbah, "Cell-free massive MIMO with limited backhaul," in *Proc. IEEE ICC*, May 2018, pp. 1–7.
- [22] D. Maryopi, M. Bashar, and A. Burr, "On the uplink throughput of zero-forcing in cell-free massive MIMO with coarse quantization," *IEEE Trans. Veh. Technol.*, pp. 1–5, Jun. 2019.
- [23] J. Tang, H. Tang, M. Cui, K. Cumanan, G. Chen, K. K. Wong, and J. A. Chambers, "Energy minimization in D2D-assisted cache-enabled internet of things: A deep reinforcement learning approach," *IEEE Trans. Ind. Electron.*, To appear.
- [24] J. Luo, J. Tang, D. So, G. Chen, K. Cumanan, and J. A. Chambers, "A deep learning based approach to power minimization in multi-carrier NOMA with SWIPT," *IEEE Access*, vol. 7, pp. 17 450–17 460, Jan. 2019.
- [25] J. Tang, H. Tang, K. Cumanan, S. Zhang, and Y. Zhou, "A reinforcement learning approach for D2D-assisted cache enabled HetNets," in *Proc. IEEE Globecom*, Oct. 2019, pp. 1–6.
- [26] W. Lee, M. Kim, and D. Cho, "Deep power control: Transmit power control scheme based on convolutional neural network," *IEEE Commun. Lett.*, vol. 22, no. 6, pp. 1276–1279, Jun. 2018.
- [27] T. V. Chien, T. N. Canh, E. Björnson, and E. G. Larsson, "Power control in cellular massive MIMO with varying user activity: A deep learning solution," [online]. Available: <https://arxiv.org/pdf/1901.03620.pdf>, pp. 1–30, 2019.
- [28] H. Sun, X. Chen, Q. Shi, M. Hong, X. Fu, , and N. D. Sidiropoulos, "Learning to optimize: Training deep neural networks for interference management," *IEEE Trans. Signal Process.*, vol. 66, no. 20, pp. 5438–5453, Oct. 2018.
- [29] T. N. Sainath, B. Kingsbury, A. R. Mohamed, G. E. Dahl, G. Saon, H. Soltan, T. Beran, A. Y. Aravkin, and B. Ramabhadran, "Improvements to deep convolutional neural networks for LVCSR," in *Proc. IEEE ASRU*, 2013, pp. 1–7.
- [30] K. Zhang, W. Zuo, Y. Chen, D. Meng, and L. Zhang, "Beyond a gaussian denoiser: Residual learning of deep CNN for image denoising," *IEEE Trans. Image Process.*, vol. 66, no. 20, pp. 5438–5453, Oct. 2018.
- [31] T. S. Rappaport, *Wireless Communications: Principles and Practice*. Englewood Cliffs, NJ, USA: Prentice-Hall, 2002.
- [32] I. Viering, H. Hofstetter, and W. Utschick, "Spatial long-term variations in urban, rural and indoor environments," in *Proc. the 5th Meeting of COST273, Lisbon, Portugal*, Sep. 2002.

- [33] T. L. Marzetta, E. G. Larsson, H. Yang, and H. Q. Ngo, *Fundamentals of massive MIMO*. Cambridge University Press, 2016.
- [34] C. D'Andrea, A. Zappone, S. Buzzi, and M. Debbah, "Uplink power control in cell-free massive MIMO via deep learning," [online]. Available: <https://arxiv.org/pdf/1908.11121.pdf>, pp. 1–5, 2019.
- [35] M. Bashar, K. Haneda, A. Burr, and K. Cumanan, "A study of dynamic multipath clusters at 60 GHz in a large indoor environment," in *Proc. IEEE Globecom Workshop*, Dec. 2018.
- [36] M. Bashar, A. G. Burr, K. Haneda, K. Cumanan, M. M. Molu, M. Khalily, and P. Xiao, "Evaluation of low complexity massive MIMO techniques under realistic channel conditions," *IEEE Trans. Veh. Technol.*, vol. 68, no. 9, pp. 9297–9302, Sep. 2019.
- [37] M. Bashar, A. G. Burr, D. Maryopi, K. Haneda, and K. Cumanan, "Robust geometry-based user scheduling for large MIMO systems under realistic channel conditions," in *Proc. IEEE EW*, May 2018, pp. 1–6.
- [38] P. Zillmann, "Relationship between two distortion measures for memoryless nonlinear systems," *IEEE Signal Process. Lett.*, vol. 17, no. 11, pp. 917–920, Feb. 2010.
- [39] J. Xu, W. Xu, J. Zhu, D. W. K. Ng, and A. Lee Swindlehurst, "Secure massive MIMO communication with low-resolution dacs," *IEEE Trans. Wireless Commun.*, vol. 67, no. 5, pp. 3265–3278, May 2019.
- [40] J. Max, "Quantizing for minimum distortion," *IEEE Trans. Inf. Theory*, vol. 6, no. 1, pp. 7–12, Mar. 1960.
- [41] A. Kakkavas, J. Munir, A. Mezghani, H. Brunner, and J. A. Nossek, "Weighted sum rate maximization for multiuser MISO systems with low resolution digital to analog converters," in *Proc. IEEE WSA*, Mar. 2016.
- [42] A. Mezghani and J. A. Nossek, "Capacity lower bound of MIMO channels with output quantization and correlated noise," in *Proc. IEEE ISIT*, Aug. 2012, pp. 1–5.
- [43] S. P. Boyd, S. J. Kim, A. Hassibi, and L. Vandenbarghe, "A tutorial on geometric programming," *Optim. Eng.*, vol. 8, no. 1, pp. 67–128, 2007.
- [44] E. Björnson, J. Hoydis, and L. Sanguinetti, *Massive MIMO Networks: Spectral, Energy, and Hardware Efficiency*. Foundations and Trends in Signal Processing, 2017.
- [45] E. Björnson and E. Jorswieck, *Optimal Resource Allocation in Coordinated Multi-Cell Systems*. Foundations and Trends in Communications and Information Theory, 2012.
- [46] CVX Research, *Matlab Software for Disciplined Convex Programming*. Online: [cvxr.com/cvx](http://cvxr.com/cvx).
- [47] K. He, X. Zhang, S. Ren, and J. Sun, "Deep residual learning for image recognition," in *Proc. IEEE CVPR*, Jun. 2016, pp. 770–778.
- [48] Y. Nesterov and A. Nemirovsky, *Interior-point polynomial methods in convex programming*. Studies in Applied Mathematics, SIAM, Philadelphia, 1994.
- [49] S. Boyd and L. Vandenberghe, *Convex Optimization*. Cambridge, UK: Cambridge University Press, 2004.



**Manijeh Bashar** (S'16–M'20) received the B.Sc. degree in electrical engineering from the University of Guilan, Iran, in 2009, and the M.Sc. degree in communication systems engineering (with honors) from the Shiraz University of Technology, Iran, in 2013. She received the Ph.D. degree in communications engineering from the University of York, U.K. in 2019. In 2017, she was an Academic Visitor with the Department of Electronics and Nanoengineering, Aalto University, Espoo, Finland, with a Short Term Scientific Mission (STSM) Scholarship Award from European COST-IC1004 "Cooperative Radio Communications for Green Smart Environments".

She is currently a research fellow at the Institute for Communication Systems (ICS), the Home of 5G Innovation Centre (5GIC), University of Surrey. Her current research interests include cooperative communications for 5G networks including distributed massive MIMO, Cloud-RAN, Fog-RAN, NOMA, deep learning, resource allocation, and also millimetre-wave channel modelling.

She received the K. M. Stott Prize for excellent Ph.D. research in electronics engineering from the University of York, U.K. in 2019. She has been awarded First place (based on jury) in the IEEE WCNC'18 three-minute Ph.D. thesis competition for her research in cell-free massive MIMO. She has been nominated for Departmental Prize for Excellence in Research in 2019 at the University of Surrey. She has been a member of Technical Program Committees (TPC) for the IEEE ICC 2020.



**Ali Akbari** (M'15) received the MSc degree in Electrical Engineering from the Shiraz University of Technology, Iran in 2012 and the PhD degree in Telecommunications from the Sorbonne Université, Paris, France in March 2018. Since July 2018, he joined the Centre for Vision, Speech and Signal Processing (CVSSP), University of Surrey, UK as a research fellow to enrich his experiences in the field of face recognition. He has published two book chapters and several papers in peer-reviewed journals and conference proceedings. He has served as an Associate Editor for the IEEE Open Journal of Circuits and Systems. His research interests include computer vision, deep learning, dictionary learning and image and video coding.



**Dr. Cumanan** (M'10–SM'19) received the BSc degree with first class honors in electrical and electronic engineering from the University of Peradeniya, Sri Lanka in 2006 and the PhD degree in signal processing for wireless communications from Loughborough University, Loughborough, UK, in 2009.

He is currently a lecturer at the Department of Electronic Engineering, The University of York, UK. From March 2012 to November 2014, he was working as a research associate at School of Electrical and Electronic Engineering, Newcastle University, UK. Prior to this, he was with the School of Electronic, Electrical and System Engineering, Loughborough University, UK. In 2011, he was an academic visitor at Department of Electrical and Computer Engineering, National University of Singapore, Singapore. From January 2006 to August 2006, he was a teaching assistant with Department of Electrical and Electronic Engineering, University of Peradeniya, Sri Lanka. His research interests include non-orthogonal multiple access (NOMA), cell-free massive MIMO, physical layer security, cognitive radio networks, convex optimization techniques and resource allocation techniques. He has published more than 80 journal articles and conference papers which attracted more than 1200 Google scholar citations. He has been also recently appointed as an associate editor for IEEE Access journal.

Dr. Cumanan was the recipient of an overseas research student award scheme (ORSAS) from Cardiff University, Wales, UK, where he was a research student between September 2006 and July 2007.



**Alister Burr** was born in London, U.K. in 1957. He received the BSc degree in Electronic Engineering from the University of Southampton, U.K. in 1979 and the PhD from the University of Bristol in 1984. Between 1975 and 1985 he worked at Thorn-EMI Central Research Laboratories in London. In 1985 he joined the Department of Electronics (now Electronic Engineering) at the University of York, U.K., where he has been Professor of Communications since 2000. His research interests are in wireless communication systems, especially MIMO,

cooperative systems, physical layer network coding, and iterative detection and decoding techniques. He has published around 250 papers in refereed international conferences and journals, and is the author of “Modulation and Coding for Wireless Communications” (published by Prentice-Hall/PHEI), and co-author of “Wireless Physical-Layer Network Coding (Cambridge University Press, 2018). In 1999 he was awarded a Senior Research Fellowship by the U.K. Royal Society, and in 2002 he received the J. Langham Thompson Premium from the Institution of Electrical Engineers. He has also given more than 15 invited presentations, including three keynote presentations. He was chair, working group 2, of a series of European COST programmes including IC1004 “Cooperative Radio Communications for Green Smart Environments” (which have been influential in 3GPP standardisation), and has also served as Associate Editor for IEEE Communications Letters, Workshops Chair for IEEE ICC 2016, and TPC co-chair for PIMRC 2018.



**Pei Xiao** is currently a Professor of wireless communications with the Institute for Communication Systems (ICS), the Home of 5G Innovation Centre (5GIC), University of Surrey. He is the Technical Manager of 5GIC, leading the research team in the new physical layer work area, and coordinating/supervising research activities across all the work areas within 5GIC. Prior to this, he was with Newcastle University and Queen’s University Belfast. He also held positions at Nokia Networks, Finland. He has published extensively in the fields of communication theory, RF and antenna design, and signal processing for wireless communications. He is an inventor of over 10 recent 5GIC patents and addressing bottleneck problems in 5G systems.



**Mérouane Debbah** (S’01–M’04–SM’08–F’15) received the M.Sc. and Ph.D. degrees from the Ecole Normale Supérieure Paris-Saclay, France. He was with Motorola Labs, Saclay, France, from 1999 to 2002, and also with the Vienna Research Center for Telecommunications, Vienna, Austria, until 2003. From 2003 to 2007, he was an Assistant Professor with the Mobile Communications Department, Institut Eurecom, Sophia Antipolis, France. In 2007, he was appointed Full Professor at CentraleSupélec, Gif-sur-Yvette, France. From 2007 to 2014, he was

the Director of the Alcatel-Lucent Chair on Flexible Radio. Since 2014, he has been Vice-President of the Huawei France Research Center. He is jointly the director of the Mathematical and Algorithmic Sciences Lab as well as the director of the Lagrange Mathematical and Computing Research Center. He has managed 8 EU projects and more than 24 national and international projects. His research interests lie in fundamental mathematics, algorithms, statistics, information, and communication sciences research. He is an IEEE Fellow, a WWRF Fellow, and a Membre émérite SEE. He was a recipient of the ERC Grant MORE (Advanced Mathematical Tools for Complex Network Engineering) from 2012 to 2017. He was a recipient of the Mario Boella Award in 2005, the IEEE Glavieux Prize Award in 2011, the Qualcomm Innovation Prize Award in 2012 and the 2019 IEEE Radio Communications Committee Technical Recognition Award. He received 20 best paper awards, among which the 2007 IEEE GLOBECOM Best Paper Award, the Wi-Opt 2009 Best Paper Award, the 2010 Newcom++ Best Paper Award, the WUN CogCom Best Paper 2012 and 2013 Award, the 2014 WCNC Best Paper Award, the 2015 ICC Best Paper Award, the 2015 IEEE Communications Society Leonard G. Abraham Prize, the 2015 IEEE Communications Society Fred W. Ellersick Prize, the 2016 IEEE Communications Society Best Tutorial Paper Award, the 2016 European Wireless Best Paper Award, the 2017 Eurasiap Best Paper Award, the 2018 IEEE Marconi Prize Paper Award, the 2019 IEEE Communications Society Young Author Best Paper Award and the Valuetools 2007, Valuetools 2008, CrownCom 2009, Valuetools 2012, SAM 2014, and 2017 IEEE Sweden VT-COM-IT Joint Chapter best student paper awards. He is an Associate Editor-in-Chief of the journal *Random Matrix: Theory and Applications*. He was an Associate Area Editor and Senior Area Editor of the IEEE TRANSACTIONS ON SIGNAL PROCESSING from 2011 to 2013 and from 2013 to 2014, respectively.



**Hien Quoc Ngo** received the B.S. degree in electrical engineering from the Ho Chi Minh City University of Technology, Vietnam, in 2007, the M.S. degree in electronics and radio engineering from Kyung Hee University, South Korea, in 2010, and the Ph.D. degree in communication systems from Linköping University (LiU), Sweden, in 2015. In 2014, he visited the Nokia Bell Labs, Murray Hill, New Jersey, USA. From January 2016 to April 2017, Hien Quoc Ngo was a VR researcher at the Department of Electrical Engineering (ISY), LiU.

He was also a Visiting Research Fellow at the School of Electronics, Electrical Engineering and Computer Science, Queen’s University Belfast, UK, funded by the Swedish Research Council.

Hien Quoc Ngo is currently a Lecturer at Queen’s University Belfast, UK. His main research interests include massive (large-scale) MIMO systems, cell-free massive MIMO, physical layer security, and cooperative communications. He has co-authored many research papers in wireless communications and co-authored the Cambridge University Press textbook *Fundamentals of massive MIMO* (2016).

Dr. Hien Quoc Ngo received the IEEE ComSoc Stephen O. Rice Prize in Communications Theory in 2015, the IEEE ComSoc Leonard G. Abraham Prize in 2017, and the Best PhD Award from EURASIP in 2018. He also received the IEEE Sweden VT-COM-IT Joint Chapter Best Student Journal Paper Award in 2015. He was an *IEEE Communications Letters* exemplary reviewer for 2014, an *IEEE Transactions on Communications* exemplary reviewer for 2015, and an *IEEE Wireless Communications Letters* exemplary reviewer for 2016. He was awarded the UKRI Future Leaders Fellowship in 2019. Dr. Hien Quoc Ngo currently serves as an Editor for the IEEE Wireless Communications Letters, Digital Signal Processing, and IEICE Transactions on Fundamentals of Electronics, Communications and Computer Sciences. He was a Guest Editor of IET Communications, special issue on “Recent Advances on 5G Communications” and a Guest Editor of IEEE Access, special issue on “Modelling, Analysis, and Design of 5G Ultra-Dense Networks”, in 2017. He has been a member of Technical Program Committees for several IEEE conferences such as ICC, GLOBECOM, WCNC, and VTC.



**Josef Kittler** (PhD, ScD) is Professor of Machine Intelligence at the Centre for Vision, Speech and Signal Processing, Department of Electronic Engineering, University of Surrey. He conducts research in biometrics, video and image database retrieval, and cognitive vision. He published a Prentice Hall textbook on Pattern Recognition: A Statistical Approach, and more than 300 journal papers. He serves on the Editorial Board of several journals in Pattern Recognition and Computer Vision.